JGR Solid Earth

RESEARCH ARTICLE
10.1029/2025JB031995

Constraints on Magma Pressure Distribution During Long Range Lateral Propagation of Giant Radial Dyke Swarms

M. Foschi[1] and **J. A. Cartwright**[1]

[1]Department of Earth Sciences, University of Oxford, Oxford, UK

Key Points:

- Sill intrusions were used as pressure piezometers to reconstruct paleo-pressure along the giant Mull Dyke Swarm
- The concept of a level of neutral buoyancy fails to predict the upper tip depth of this giant dyke swarm
- Near-surface magma cooling is proposed to explain both the lateral propagation of the dyke swarm and the suppression of eruption along its trajectory

Supporting Information:

Supporting Information may be found in the online version of this article.

Correspondence to:

M. Foschi,
martino.foschi@earth.ox.ac.uk

Citation:

Foschi, M., & Cartwright, J. A. (2025). Constraints on magma pressure distribution during long range lateral propagation of giant radial dyke swarms. *Journal of Geophysical Research: Solid Earth*, *130*, e2025JB031995. https://doi.org/10.1029/2025JB031995

Received 14 MAY 2025
Accepted 24 SEP 2025

Author Contributions:

Conceptualization: M. Foschi, J. A. Cartwright
Data curation: J. A. Cartwright
Formal analysis: M. Foschi, J. A. Cartwright
Investigation: M. Foschi, J. A. Cartwright
Methodology: M. Foschi, J. A. Cartwright
Software: M. Foschi
Validation: J. A. Cartwright
Visualization: M. Foschi
Writing – original draft: M. Foschi, J. A. Cartwright
Writing – review & editing: M. Foschi, J. A. Cartwright

Abstract Giant dyke swarms are important but enigmatic components of magma transport in the Earth and terrestrial planets. Although widely documented on Earth, Venus, and Mars as extending laterally for 100–1,000 s of kilometers from their magma sources, the reasons for this extraordinary lateral propagation are not known. A critical parameter in dyke propagation is magma pressure, but this is generally unknown. This uncertainty is a barrier to improve physical modeling and prediction of volcanic hazards. Here, we combined rock mechanical analyses with geological constraints from the largest dykes of the giant Mull Dyke Swarm to reconstruct magma pressures using a Monte Carlo framework at six locations along the 660 km long trajectory of the dykes. Our results show that in the most conservative of our scenarios the magma pressures were sufficiently high for the dykes to erupt 100 s km from the magma source. Moreover, we show that magma depressurization over distance is crudely exponential and not linear as previously thought. We also argue that the concept of the level of neutral buoyancy fails to predict the upper termination depth of Mull dykes by several kilometers. We argue that near-surface cooling played a crucial role in maintaining dyke tips beneath the surface hence promoting long range propagation.

Plain Language Summary Giant dyke swarms are some of the largest, yet least-understood volcanic features on Earth, Venus or Mars. These dykes are rock fissures which can be as much as 2,000 km long, 100 m wide and extend deeper than 50 km. They carry significant amounts of molten rock which travels sideways, for extensive distances, rather than flowing out at the surface as with volcanoes and lava flows. The big question is, why do they do this? As these dykes are the biggest movers and shakers of the molten rock world, we need to answer this question if we are going to be able to predict volcanic eruptions accurately. We studied a 58 million year old dyke swarm in Britain and, using multi-sourced geological information, we modeled the pressure within these propagating dykes. This showed that they ought to have erupted but when the fissures approached the surface and met cold groundwater, this cooled the molten rock and prevented eruption. If you imagine dropping molten metal into a bucket of cold water, this will cause a release of steam and the metal (here, molten rock) will cool and freeze. We argue that the same process was responsible for preventing eruptions from the dyke swarms.

1. Introduction

Giant dyke swarms are important components of magmatic plumbing systems capable of transporting huge volumes of magma vertically and laterally over large distances and feed flood basalt provinces with very large magma fluxes (Ernst et al., 1995; Fialko & Rubin, 1999; Magee et al., 2019). Giant dyke swarms are developed widely on Earth and are also inferred to occur widely on Venus and Mars (Ernst et al., 1995, 2001; Head & Wilson, 1992; Scott et al., 2002; Srivastava et al., 2019; Wilson & Head, 2002). Over 150 giant dyke swarms have been documented on Earth and over 400 on Venus and Mars (Ernst et al., 2001). Individual dykes are commonly >100 km long and exceptionally >1,000 km long (El Bilali & Ernst, 2024). Their structure is poorly constrained due to erosion after their emplacement and the lack of high-resolution sub-surface imaging methods means that some key aspects of the emplacement of giant dyke swarms remain enigmatic. Specifically, it is not known how and why individual dykes in the swarms are able to propagate laterally for 100–1,000 s km without magma erupting at surface (Ernst et al., 1995; Fialko & Rubin, 1999; Parfitt & Head, 1993; Pinel & Jaupart, 2004; Rubin & Pollard, 1987). Establishing what factors control lateral propagation is important for all laterally propagating dykes because they are an intrinsic component of many magmatic plumbing systems, but particularly challenging for giant dyke swarms due to the large dimensions involved and the observation that giant dykes transect radically varying crustal domains (Ernst et al., 1995).

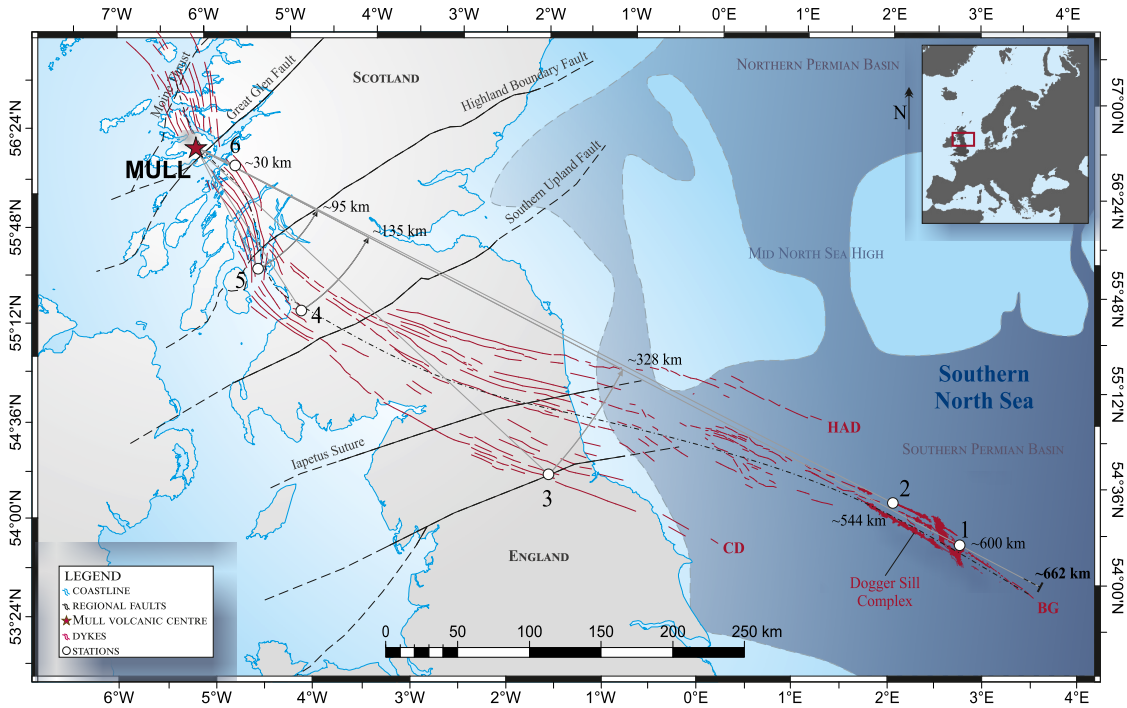

Figure 1. Location of the Mull Volcanic Center which consists of three aligned, closely spaced sub-centers (Kerr et al., 1999), the Mull Dyke Swarm (onshore dyke traces are from the British Geological Survey 1:250,000 sheets of N. England and S. Scotland; offshore dyke traces are from Carver et al., 2023) the Dogger Sill Complex (from Cartwright et al., 2025), and the position of the Stations 1–6 (see text). The Mull Dyke Swarm extends to the SE into the Southern Permian Basin for about 660 km and intersects a number of regional faults (black continuous and dashed lines). Cleveland Dyke = CD; Blyth Group = BG; Hawick-Acklington Group = HAG (from Carver et al., 2023).

A number of theoretical modeling studies have analyzed what delimits the lateral propagation of dykes. Key factors include (a) declining magma pressure at the source reservoir, (b) mechanical barriers (stress and strength barriers), (c) magma pressure loss during transport or (d) cooling of the magma (Buck et al., 2006; Delaney & Pollard, 1982; Gudmundsson, 2020; Maccaferri et al., 2016; Rivalta et al., 2015; Rubin & Pollard, 1987). However, for giant dyke swarms the source pressure is an unknown, as is the pressure distribution within the propagating dyke. Source magma pressures are generally estimated from consideration of failure criteria in the walls of the magma chamber that is assumed to represent the source (to calculate the conditions required for lateral propagation (e.g., Grosfils, 2007; Gudmundsson, 2012; McLeod & Tait, 1999; Pinel & Jaupart, 2003; Rivalta, 2010; Townsend et al., 2017)). Similarly, pressure losses during transport are difficult or even impossible to quantify, with assumptions typically made for fracture roughness, dyke dimensions, host rock compressibility and propagation velocity, with either constant flux or source pressure boundary conditions (Lister & Kerr, 1991; Rubin, 1995; Rubin & Pollard, 1987).

In all of these theoretical models, assumptions are made about magma pressure that favor either the intrinsic fluid dynamical or rock mechanical emphasis in the formulation of the problem and its solution (Lister & Kerr, 1991; Rivalta et al., 2015; Rubin, 1995; Townsend et al., 2017). However, the lack of constraint on magma pressure distribution in dykes means that these models are not adequately tested and a multiplicity of contrasting factors explaining lateral propagation remain in play.

Here we aim to provide constraints for magma pressure in a laterally propagating dyke that are derived using an approach based on the analysis of fluid pressure driven fractures. We apply this to a mechanical analysis of dyke and sill intrusions comprising one of the best documented terrestrial giant dyke swarms, the Mull Dyke Swarm (MDS) (Carver et al., 2023) (Figure 1). We reconstruct lower bounds for magma pressure at widely separated localities along the trajectory of two of the major dykes within the swarm by computing minimum pressure values necessary to form sills at shallow levels in the crust which were demonstrably fed by the dykes. Sills are ideal piezometers, providing rock mechanical parameters are well known, and we demonstrate their potential utility for

reconstructing the pressure in magmatic plumbing systems more generally. We use the pressure constraints derived from analyzing conditions for both dyke and sill propagation to critically evaluate existing mechanisms cited as explanation for the extraordinary lateral propagation of giant dyke swarms.

1.1. The Mull Dyke Swarm

The Mull Dyke Swarm (MDS) was emplaced in the Paleocene during the later stages of the main period of igneous activity in the Hebridean igneous province of NW Scotland (Kerr et al., 1999). The dyke swarm is oriented broadly NW-SE, orthogonal to the newly opening NE Atlantic Ocean in a bilateral configuration from a sub-volcanic source reservoir beneath the island of Mull, one of the main igneous centers for the Hebridean Magmatic Province (Bailey, 1924; Horni et al., 2017; Kerr et al., 1999; Saunders et al., 1997; Thompson et al., 1986). Geochemical modeling of dyke magmas has demonstrated that the sub-volcanic source consisted of two distinct magma reservoirs, a shallow chamber at c. 7–8 km and a deeper one at or close to the Moho (Ishizuka et al., 2017; Macdonald et al., 2010, 2015; Morrison et al., 1985).

The MDS consists of hundreds of individual dykes intruded in an approximately NW-SE zone some tens of kilometers wide with its locus in the three aligned sub-volcanic centers on Mull (Figure 1) (Geikie, 1897; Jolly & Sanderson, 1995; Richey, 1939; Tyrrell, 1917). Three sub-swarms consisting of a small number of the largest individual dykes extend furthest to the ESE from Mull, crossing major crustal domain boundaries (Beamish et al., 2016) with little deviation from their curvilinear trajectory as they follow the regional stress field (Carver et al., 2023; England, 1988).

The southern sub-swarm includes the Cleveland Dyke, which terminates just off the coast of NE England, 450 km from Mull and is reported to range in width from 6 to 28 m in width at various positions along its outcrop (Macdonald et al., 1988). The central, "Blyth" sub-swarm extends furthest from Mull, with two major dykes terminating 650 and 672 km from Mull, making them amongst the longest continuously mapped dykes on Earth (Carver et al., 2023). The dykes of the Blyth sub-swarm range in thickness from 1 to 14 m at outcrop or as intersected in coal mines (Land, 1974). The dykes are all negatively magnetized and from a synthesis of Ar-Ar dating of extrusive and intrusive components of the Mull Center, it has been argued convincingly that all the igneous activity occurred between c. 61 and 58 Ma, within Chron C26R (Chambers & Pringle, 2001; Dagley et al., 2008; Kerr et al., 1999). Limited direct radiometric dating has yielded K-Ar dates of 58.4 ± 1.1 Ma (Evans et al., 1973) and 59.3 ± 2.0 Ma (Mitchell et al., 1989). Biostratigraphic dating of tuffs and tephra aprons associated with the Blyth sub-swarm yields dates of between 58 and 59 Ma (Pryce et al., 2025). These three sub-swarms therefore most likely represent three separate major intrusive events during Chron 26R, over a period of perhaps 1–3 million years. Intrusive volumes for these three events range from c. 100 to c. 200 km^3 (based on an assumed depth to the base of the constituent dykes of 10 km from Macdonald et al., 1988) implying an almost complete evacuation of the sub-volcanic reservoir, expressed in the remains of the volcanic superstructure as c. 5–8 km diameter calderas (Carver et al., 2023).

Sills have been reported previously along the MDS from outcrops, wells, seismic and aeromagnetic data (Cartwright et al., 2025; Eyles et al., 1931; Gauer et al., 2004; Mills et al., 1976; Mykura et al., 1967; Smellie, 1915; Wall et al., 2010). The most distal of these, at over 500 km from Mull, is a large sill complex, termed the Dogger Sill Complex (Figure 1). This comprises six sills covering an area of c. 400 km^2 emplaced with a mean thickness of c. 50 m within a Late Permian evaporite sequence (Cartwright et al., 2025). Smaller sills (<1 km^2) have been reported intruding into Late Carboniferous coal-bearing sequences in the coalfields of northern England, fed from the Cleveland Dyke (Mills et al., 1976). Also fed from the same dyke, but more proximally to its source on Mull, the Prestwick-Mauchline Sill Complex and the Bute Sill were intruded at shallow level into Late Carboniferous—Early Permian sequences preserved within the Midland Valley Rift (Mykura et al., 1967; Smellie, 1915). These sills are the focus of the current study since their geological context is well documented, allowing the key mechanical parameters governing their emplacement to be constrained.

Of particular interest for this study are any constraints on the depth to the upper tips for the dykes within the MDS. Constituent dykes of the MDS exposed on land in Scotland and Northern England have been subject to considerable erosion since their emplacement so it is not possible to constrain their original depth below the surface. However, upper tip positions are reasonably well constrained for the three major dykes mapped using subsurface data in the South Permian Basin (SPB) (Pryce et al., 2025; Wall et al., 2010). Phreatomagmatic eruptions have been demonstrated above the dyke tips and shown to result in chains of craters excising up to 200–

Table 1
Symbols and Parameters Used in the Text, the Figures, and in the Equations

Symbol	Description
A	Area, sill (see Equation 2)
g	Acceleration due to gravity (see Equation 2)
h	Sill thickness (see Equation 2)
H	Overburden thickness (see Equation 2)
m.s.l.	Mean sea level (see Figures 3–5, and 8, 4, 5, 8, and 11)
Ma	Mega annum
P	Pressure (see Equation 1)
P_{DYKE}	Pressure, dyke (see Figure 3)
P_M	Pressure, magma (see Figure 3)
P_{SILL}	Pressure, sill (see Figure 3)
$P0$	Pressure, dyke at $Z = 0$ (see Figure 3)
T	Tensile strength (see Equation 1)
w	Work (see Equation 2)
Z	Depth
Z_{DYKE}	Depth, dyke (see Figure 3)
$Z0$	Depth, dyke at $P = 0$ (see Figure 3)
σ_{min}	Stress, minimum (see Equation 1)
σ_1	Stress, maximum principal
σ_2, σ_3	Stress, minimum
σ_V	Stress, vertical
σ_{Hmin}	Stress, minimum horizontal
ρ	Density (see Equation 2)

300 m of the Chalk Group sediments, implying that upper dyke tips were generally located below this depth beneath the sediment surface. A 5 m wide dyke was intersected in well 44/24b-A4 at a depth below the paleo-surface of c. 700 m (Cartwright et al., 2025), so the upper tip was therefore shallower than this depth. Aeromagnetic modeling of upper tip depths ranges from 200 to 500 m below the Top Chalk reference datum (Brown et al., 1994; Gauer et al., 2004; Kirton & Donato, 1985; Wall et al., 2010) also consistent with the upper termination of seismic disturbance zones linked to the presence of vertical to sub-vertical dykes (Carver et al., 2023; Underhill, 2009).

2. Rationale and Methodology for Pressure Reconstruction

2.1. Conditions for Sill Formation

The occurrence of sills fed by the dykes within the swarm is the key which allows us to reconstruct the magma pressure in the dykes at various positions along their lateral trajectory. We adopted a conservative approach by simply addressing the specific pressure conditions required to emplace the sills. By assuming that the magma pressure at any depth within a dyke-fed sill must be equal to the magma pressure in the feeder dyke at that depth, it is possible to use the sill as a local piezometer to constrain the pressure in the dyke.

The calculation of the magma pressure necessary for sill formation is based on the standard conditions for propagation of pressure driven fractures (Engelder et al., 1990; Lister & Kerr, 1991; Pollard, 1973; Pollard & Holzhausen, 1979; Secor & Pollard, 1975). The magma pressure at the junction between dykes and sills was calculated using the standard condition for sill propagation:

$$P = \sigma_{\mathrm{min}} + T \tag{1}$$

where P is magma pressure, σ_{min} is the total confining stress perpendicular to the sill contact, and where T is the tensile strength of the host rock (see also Table 1). Since the sills intruded along bedding planes that were sub-horizontal σ_{min} is taken as being equal to σ_V (lithostatic).

The regional stress regime across the >660 km transect of the MDS is poorly constrained for the Late Paleocene with some evidence of a N-S compressional regime in parts of northern England (Hibsch et al., 1995). This conflicts with other evidence for active extension in Scotland in the area surrounding the Mull Center (England, 1988). We assume that the regional stress state during dyke propagation was with the vertical stress (lithostatic) equivalent to σ_1. The major dykes of the MDS that fed the various sills along route followed trajectories defined by the maximum horizontal compressive stress, σ_{Hmax}, which is taken as σ_2 (Carver et al., 2023; England et al., 1993), with σ_3 horizontal and orthogonal to the dykes, σ_{Hmin}.

In the reconstructions we assume that the state of stress was anisotropic over the entire vertical extent of the dykes, with the differential stress ($\sigma_V - \sigma_{\mathrm{Hmin}}$) increasing with depth. This assumption is consistent with compilations of the differential stress variation with depth in the continental crust (Behr & Platt, 2011; Burov & Watts, 2006; Townend & Zoback, 2000; Zoback et al., 2007). The minimum compressive stress (σ_{Hmin}) was taken to range from $0.7 \cdot \sigma_V$ to $0.9 \cdot \sigma_V$ (Du Rouchet, 1981). For the more distal part of the dyke trajectory this range of values fits the scatter in measurements of σ_{Hmin} made in c. 100 boreholes in the southern North Sea using leak-off tests or extended leak-off tests (Williams et al., 2015). These measurements cover the range of lithologies transected by dykes of the MDS down to depths of c. 6 km and thus provide a reasonable constraint on the variation of differential stress with depth for the final 200–300 km of dyke length. The differential stress at greater depths is a major unknown particularly in the crystalline basement lithologies transected by the dykes closer to their source on Mull. Deep borehole measurements in basement rocks show that large differential stresses of >100 MPa could be expected down to 8–10 km depth in crystalline crust (Ahlers et al., 2021; Brudy et al., 1997).

For fluid pressure-driven fractures such as sills or dykes, propagation will occur when the stress intensity factor at the tip exceeds the fracture toughness (Rubin, 1995; Rubin & Pollard, 1987; Secor & Pollard, 1975). Since the stress intensity factor scales with fracture dimensions it is typically assumed that fracture toughness (effective tensile strength) decreases to zero once the propagating fracture exceeds a length of several hundred meters (Fialko and Rubin, 1999; Lister & Kerr, 1991). However, it is necessary to assign a range of tensile strength values to account for the initial stages of propagation of the sills away from their contact with their feeder dykes using values appropriate for host rock lithologies (Table S1 in Supporting Information S1).

The inflationary stage of sill evolution involves considerable work done against the overburden load, σ_V. This work done (w) requires an additional component to the magma pressure which is given by:

$$w = \rho g h, \tag{2}$$

where, ρ is the density of the overburden, g is the acceleration due to gravity, h is the sill thickness. The work w is then divided by the volume of the overburden to convert it to the pressure P_w, via $P_w = w/HA$, where H is the thickness of the overburden, and A is the area of the sill local to the station. To account for the possibility that not all the sill thickness was achieved by hydraulic elevation of the overburden, our computations assumed a range for w using values for h from 1 m to the observed sill thickness (Table 2). The resulting equation for sill emplacement pressure, or P_{SILL}, is defined as

$$P_{\mathrm{SILL}} = \sigma_V + T + P_w \tag{3}$$

For assessment of the pressure conditions under which dyke propagation could occur, we assumed that magma pressure must be greater than the remote stress acting normal to the dyke walls (σ_{Hmin}) (Rubin, 1995) and neglected any tensile strength (Equation 1). We consider that the dyke lengths are large enough for the fracture toughness to be close to zero at the dyke tips (cf. Rubin, 1995). This magma pressure condition for continued dyke propagation is equivalent to the fracture opening pressure of Hubbert and Willis (1957) and does not take account of the work done by the magma pressure to open a significant aperture fracture against the rock compressibility. As discussed below, this approach is conservative and results in dyke tip depths which are deeper than if we simply assumed that dykes develop once magma pressure exceeds the lithostatic stress as is commonly the case in analytical treatments (e.g., Walker, 1989).

2.2. Methodology for Pressure Reconstruction and Parameterization

2.2.1. Depth of Major Lithological Units

To reconstruct the magma pressure required to form the sills identified along the trajectory of the MDS it was necessary to reconstruct the emplacement depth of the sills at the time of intrusion. For the onshore region, this necessitated estimation of the amount of post-emplacement erosion that has occurred. For the offshore region where there has been almost continuous burial since the time of intrusion, it was necessary to assess the amount of compaction of the sedimentary units above the sills so that present day thicknesses of different sedimentary units could be restored to their appropriate values at the time of intrusion (Figure 2a). Both the onshore and offshore reconstructions yielded significant ranges of values for sill depths Z and for all the depths to major lithological boundaries reflecting inherent uncertainties in erosional magnitudes and decompaction parameters (Table 2). The uncertainties due to decompaction used as inputs into the pressure reconstructions were maximum values from previous analyses of compactional strain in accordance with our aim of taking a conservative approach.

Major rock units were defined based on dominant lithologies and following local stratigraphic definitions. The boundaries between rock units with different average densities were given a range and a probability distribution function based on assessing the specific methods used to reconstruct the depths of these boundaries at the time of intrusion (Text S1 in Supporting Information S1). The sill depth and thickness are plotted at their reconstructed depth at the time of emplacement, and this depth varies as a function of the depth range applied to the host rock unit.

For the analysis of sills identified in localities onshore (Figure 1), reconstruction of the overburden at the time the sills were intruded was undertaken by constructing regional geological sections from areas of nearest preserved overburden and extrapolating to the chosen locations (Figure 2b). These sections were then restored to their Late

Journal of Geophysical Research: Solid Earth
10.1029/2025JB031995

Table 2
Location and Parameters Used to Calculate the Depth, the Pressure and the Stress for Station 1–6 (See Figure 1 for Station Location) (See Text S1 in Supporting Information S1 for Further Information on Geological Reconstruction of the Sill Locations)

Location	Property	Parameter	Units	Min	Max	Mean	STD	References
Station 1 (Dogger Sill Complex; 44/24A-5)	Thickness	Water column	m	100	300	200	57	Cameron et al. (1992); Lott and Knox (1994)
		Claystone and chalk		640	1,000	800	180	Fabricius (2003, 2007)
		Triassic and Jurassic		1,000	1,500	1,225	250	Well 44/24A-5; Mondol et al. (2008)
		Zechstein Salt		1	70	8	34.5	Hughes and Davison (1993); Stewart and Coward (1995)
		Sill		45	45	45	0	Well 44/24A-5
		Zechstein Salt		345	375	360	15	Hughes and Davison (1993); Stewart and Coward (1995)
		Permian and Carboniferous		4,800	4,850	4,825	25	Kimbell and Williamson (2015); Fairhead et al. (2023)
		Crystalline basement		3,000	1,500	2,121	750	Blundell (1993); Rijkers et al. (1993)
	Density	Sea water	$kg{\cdot}m^{-3}$	1,010	1,030	1,020	10	Mavko et al. (2020)
		Claystone and chalk		2,100	2,300	2,198	100	Well 44/24A-5
		Triassic and Jurassic		2,300	2,500	2,398	100	Kimbell and Williamson (2015)
		Zechstein Salt		2,100	2,200	2,149	50	Jackson and Hudec (2017)
		Dolerite		2,900	3,100	2,998	100	Sparks et al. (1980); Murase and McBirney (1973); Ryan (1993); Gudmundsson (2020)
		Permian and Carboniferous		2,500	2,600	2,550	50	Williamson et al. (2002); Kimbell et al. (1989); Kimbell et al. (2010); Kimbell and Williamson (2015); Donato (2020); Fairhead et al. (2023)
		Crystalline basement		2,700	2,800	2,750	50	
Station 2 (Dogger Sill Complex; 44/11-3)	Thickness	Water column	m	100	300	200	57	Cameron et al. (1992); Lott and Knox (1994)
		Claystone and chalk		360	600	465	120	Fabricius (2003, 2007)
		Triassic and Jurassic		1,400	2,000	1,673	300	Mondol et al. (2008)
		Zechstein Salt		1	30	5	14.5	Hughes and Davison (1993); Stewart and Coward (1995)
		Sill		98	98	98	0	well 44/11-3
		Zechstein Salt		592	792	685	100	Hughes and Davison (1993); Stewart and Coward (1995)
		Permian and Carboniferous		4,420	4,580	4,499	80	Williamson et al. (2002); Kimbell and Williamson (2015); Fairhead et al. (2023)
		Crystalline basement		3,000	1,600	2,191	700	Blundell (1993); Rijkers et al. (1993)
	Density	Sea water	$kg{\cdot}m^{-3}$	1,010	1,030	1,020	10	Mavko et al. (2020)
		Claystone and chalk		2,100	2,300	2,198	100	well 44/11-3
		Triassic and Jurassic		2,300	2,500	2,398	100	Kimbell and Williamson (2015)
		Zechstein Salt		2,100	2,200	2,149	50	Jackson and Hudec (2017)
		Dolerite		2,900	3,100	2,998	100	Sparks et al. (1980); Murase and McBirney (1973); Ryan (1993); Gudmundsson (2020)
		Permian and Carboniferous		2,500	2,600	2,550	50	Williamson et al. (2002); Kimbell et al. (1989); Kimbell et al. (2010); Kimbell and Williamson (2015); Donato (2020); Fairhead et al. (2023)
		Crystalline basement		2,700	2,800	2,750	50	
Station 3 (The Bolam Sill, County Durham)	Thickness	Chalk	m	400	600	490	100	Land (1987); Fox-Strangeways et al. (1992)
		Perm. Triassic and Jurassic		1,700	2,100	1,889	200	
		Pre. Permian		100	200	141	50	

Journal of Geophysical Research: Solid Earth

10.1029/2025JB031995

Table 2
Continued

Location	Property	Parameter	Units	Min	Max	Mean	STD	References
		Sill		1	10	3	4.5	Mills et al. (1976)
		Permian and Carboniferous		4,790	6,090	5,401	650	Bott et al. (1984); Kimbell et al. (1989)
		Crystalline basement		3,000	1,000	1,732	1,000	
	Density	Chalk	$kg{\cdot}m^{-3}$	2,100	2,300	2,198	100	well 44/11-3
		Perm. Triassic and Jurassic		2,300	2,500	2,398	100	Williamson et al. (2002); Kimbell et al. (1989); Kimbell et al. (2010); Kimbell and Williamson (2015); Donato (2020); Fairhead et al. (2023)
		Pre. Permian		2,500	2,600	2,550	50	
		Dolerite		2,900	3,100	2,998	100	
		Permian and Carboniferous		2,500	2,600	2,550	50	
		Crystalline basement		2,700	2,800	2,750	50	
Station 4 (The Prestwick-Mauchline Sill Complex)	Thickness	Permian	m	795	770	782	12.5	Cameron and Stephenson (1985); Caldwell and Young (2013)
		Sill		10	60	24	25	
		Permian and Up. Carb		195	670	361	237.5	
		Upper Carb.		400	600	490	100	Eyles et al. (1949); Mykura et al. (1967); Cameron and Stephenson (1985)
		Lower Carboniferous		2,600	3,000	2,793	200	
		Crystalline basement		6,000	4,900	5,422	550	
	Density	Permian	$kg{\cdot}m^{-3}$	2,300	2,500	2,398	100	Williamson et al. (2002); Kimbell et al. (1989); Kimbell et al. (2010); Kimbell and Williamson (2015); Donato (2020); Fairhead et al. (2023)
		Dolerite		2,900	3,100	2,998	100	
		Permian and Up. Carb		2,350	2,550	2,448	100	
		Upper Carb.		2,500	2,600	2,550	50	
		Lower Carboniferous		2,550	2,650	2,600	50	
		Crystalline basement		2,700	2,800	2,750	50	
Station 5 (The Bute Composite Sill)	Thickness	Perm. Triassic and Jurassic	m	475	975	681	250	Smellie (1915); Evans (1985); Cameron and Stephenson (1985)
		Sill		1	25	5	12	
		Permian and Carboniferous		1,000	3,000	1,732	1,000	
		Crystalline basement		8,500	7,000	7,714	750	
	Density	Perm. Triassic and Jurassic	$kg{\cdot}m^{-3}$	2,300	2,500	2,398	100	Williamson et al. (2002); Kimbell et al. (1989); Kimbell et al. (2010); Kimbell and Williamson (2015); Donato (2020); Fairhead et al. (2023)
		dolerite		2,900	3,100	2,998	100	
		Permian and Carboniferous		2,500	2,600	2,550	50	
		Crystalline basement		2,700	2,800	2,750	50	
Station 6 (Loch Scammadale, Argyll, W Scotland)	Thickness	Lava piles	m	800	1,000	894	100	Kynaston and Hill (1908), Lee and Bailey (1925); Groome and Hall (1974)
		Dalradian Supergroup		7,200	7,000	7,099	100	Bailey (1934); Harris and Pitcher (1975)
		Lewisian Basement		3,000	3,000	3,000	0	Barton (1992)
	Density	Basalts and basaltic andesites	$kg{\cdot}m^{-3}$	2,700	2,800	2,750	50	Gudmundsson (2020)
		Schist		2,500	2,900	2,693	200	
		Crystalline basement						Blundell (1993); Rijkers et al. (1993)

Note. In the table min = minimum, max = maximum, and STD = standard deviation.

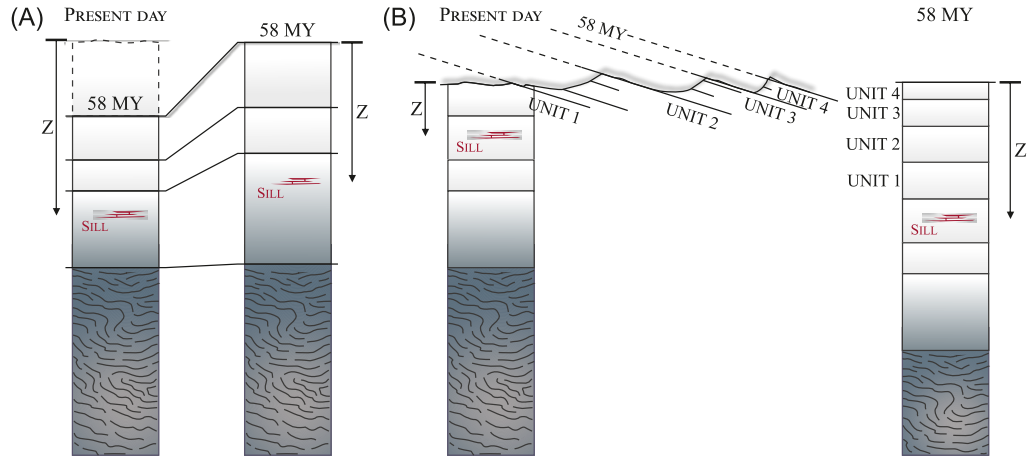

Figure 2. Schematic cartoon showing the geological reconstruction of the stratigraphic column at the time of intrusion. (a) Restoration of the units deposited after the age of the emplacement of the sills at 58 Ma with decompaction applied to restore original unit thicknesses under the reduced overburden load. (b) Simple restoration of eroded units by lateral projection from their nearest outcrop or subsurface calibration (from mine plans and/or boreholes).

Paleocene configurations using available constraints such as paleo-environmental (Gale & Lovell, 2018; Macdonald, 2024; Walsh et al., 1999) or thermal indicators of maximum burial depth (Bray et al., 1992; Green et al., 2012; Holliday, 1993).

Depth values for the boundaries of all major stratigraphic units were taken directly from published cross-sections for the onshore localities in the study and from well data for the two localities offshore within the southern Permian Basin. These latter two locations were sited at specific wells chosen for having intersected sills, and for their depth of penetration to the largest possible total depth. This gave the greatest control on sedimentary rock densities to the greatest depth extent.

For the two localities in the offshore region (Figure 1), we used present day thicknesses from well data to reconstruct the depths of stratigraphic units and intrusions in the Paleocene. Compaction under subsequent sedimentary loads was estimated from standard compaction curves for the dominant lithologies taking the maximum values for compactional strain as appropriate (Japsen, 1998; Velde, 1996; Zadeh et al., 2016). The uncertainties in reconstructing decompacted thicknesses (Waltham et al., 2000) were implicitly addressed in the large range of depth values input into the Monte Carlo framework.

2.2.2. Density of Major Lithological Units

Density values for the major lithological units were derived from a variety of published sources for the onshore region (Table 2) (see also Text S1 in Supporting Information S1). These sources provided an effective range of values reflecting the uncertainties in the methods used to obtain density values and the averaging errors involved in grouping lithologically diverse sub-units into a larger unit with a given assigned average density. For the offshore region, density values were obtained using a combination of density log data derived from wells and published density values, particularly for rock units beyond the maximum depth of penetration of the wells (Donato, 2020; Fairhead et al., 2023; Kimbell & Williamson, 2015; Kimbell et al., 2006). The uncertainty in the density values of shallow buried units principally derived from that connected to the decompaction estimation and is reflected in the large range of values selected.

Magma density was used in the reconstruction of magma pressure gradients (see below). The magma compositions of the Mull Dyke Swarm are well known and vary from basalts to basaltic andesites (Holmes & Harwood, 1929; Ishizuka et al., 2017; Kerr et al., 1999; Macdonald et al., 1988). Individual dykes of the MDS are remarkably consistent in their major element geochemistry (Macdonald et al., 2010, 2015) with low volatile components consistent with the few observations of vesicular texture in exposed dykes (Holmes & Harwood, 1929). Magma density values used in the reconstructions therefore used published values typical for the observed dyke compositions. The selected densities ranged from 2,550 to 2,750 $kg{\cdot}m^{-3}$ (Gudmundsson, 2020;

Murase & McBirney, 1973; Ryan, 1993; Sparks et al., 1980) and this large range reflects the combined uncertainties in magma composition, volatile composition and volatile exsolution during propagation (Sparks, 2003; Wilson & Head, 1981).

2.2.3. Monte Carlo Framework

To account for uncertainties in the depth and density of the main overburden units, all calculations were performed within a Monte Carlo framework (Metropolis & Ulam, 1949). In each iteration, a single value for each variable was randomly sampled from a probability distribution defined by the variable's minimum and maximum values. For each locality, the Monte Carlo framework was based on a sample size $N = 1{\cdot}10^6$. This resulted in $1{\cdot}10^6$ computations of magma pressure necessary to form the sills of observed thicknesses encompassing the ranges of density and depth used as inputs. We then computed pressure-depth relationships over a depth range between a reference datum at the reconstructed surface (mean sea level) at 58 Ma and a notional basal datum set at 10 km depth beneath this paleo-surface. The results were then plotted using standard box plots (or whisker plots). The results are then expressed in the following descriptions as the second and the third quartile (or the 25th percentile, P25, and the 75th percentile, P75).

The choice of the lower reference datum used for the pressure-depth plots of 10 km derived from the maximum height assumed for the longest dykes in the MDS in previous studies (Carver et al., 2023; Macdonald et al., 1988). This value of 10 km for the deeper datum was adopted for two reasons. Firstly, the shallow magma chamber depth below Mull believed to be the primary source of the magma feeding the dykes has been estimated to have been at a depth of 7–8 km based on evidence from crustal contamination of the dyke magma (Ishizuka et al., 2017). Downward propagation from an injection point at the lateral margins of this shallow chamber would be possible if reservoir source pressure was greater than lithostatic, and we assume this downward propagation was unlikely to exceed a few kilometers (cf. Rubin & Pollard, 1987). The magma chamber depth therefore sets an approximate basal limit to dyke propagation (Fialko & Rubin, 1999). Secondly, the propagation trajectory of the dykes is curvilinear and tracks a σ_2 direction that does not change its orientation across any of the large faults crossing the upper crustal domains apart from the Highland Boundary Fault (Figure 1) (Carver et al., 2023). This suggests that the dyke propagation directions are rooted in propagation orientation by the stress state at a depth within the crust below the level of influence of significant upper crustal mechanical heterogeneities and close to the depth where differential stress is a maximum (Zoback et al., 2007). This reasoning does not give a strict depth range but is based on the changes in differential stress that would be expected approaching the mid-crustal brittle-ductile transition.

To reconstruct pressure-depth relationships at 58 Ma, it was necessary to extrapolate the Monte Carlo simulated values for sill magma pressure upwards and downwards along the respective feeder dyke for each sill. This extrapolation used the range of static magma pressure gradients chosen to reflect the 2,550–2,750 $kg{\cdot}m^{-3}$ range in magma density. Static magma pressure gradients are typically assumed for theoretical treatments of dyke propagation simply because dynamic gradients cannot be quantified using generally available constraints (Rivalta et al., 2015; Rubin, 1995). Delaney and Pollard (1982) and Rubin and Pollard (1987) estimate the driving pressure gradient to be no more than 1% of the static gradient. The upward loss of magma pressure due to viscous forces, wall friction or constriction toward the dyke tips (Lister & Kerr, 1991; Rubin & Pollard, 1987) is factored into our Monte Carlo framework by choosing a deliberately broad range for magma density.

The aim of the extrapolation was to compute how the magma pressure varied vertically within the dyke using a conservative assumption that its pressure was fixed at the sill pressure where dyke and sill intersected. The upward extrapolation was undertaken specifically to test whether there was sufficient magma pressure in the dyke to result in eruption given the constraint of a known and verified sill intrusion. The downward extrapolation was aimed at assessing the lateral variation in the magma pressure in the dyke at a reference level considered to be close to the base of the dyke.

To illustrate the approach taken in the extrapolation of magma pressure within the feeder dyke, three hypothetical pressure depth plots are shown in Figure 3. The first example (Figure 3a) shows a situation where the magma pressure in the sill at depth Z is the maximum within the range allowed, with maximum values of tensile strength (T) and work done to inflate the sill (w). Extrapolating the magma pressure upwards using the minimum magma density results in a positive intersection of magma pressure at the surface datum at mean sea level, implying a surface eruption should occur. Magma pressure would project to zero at some height above the surface

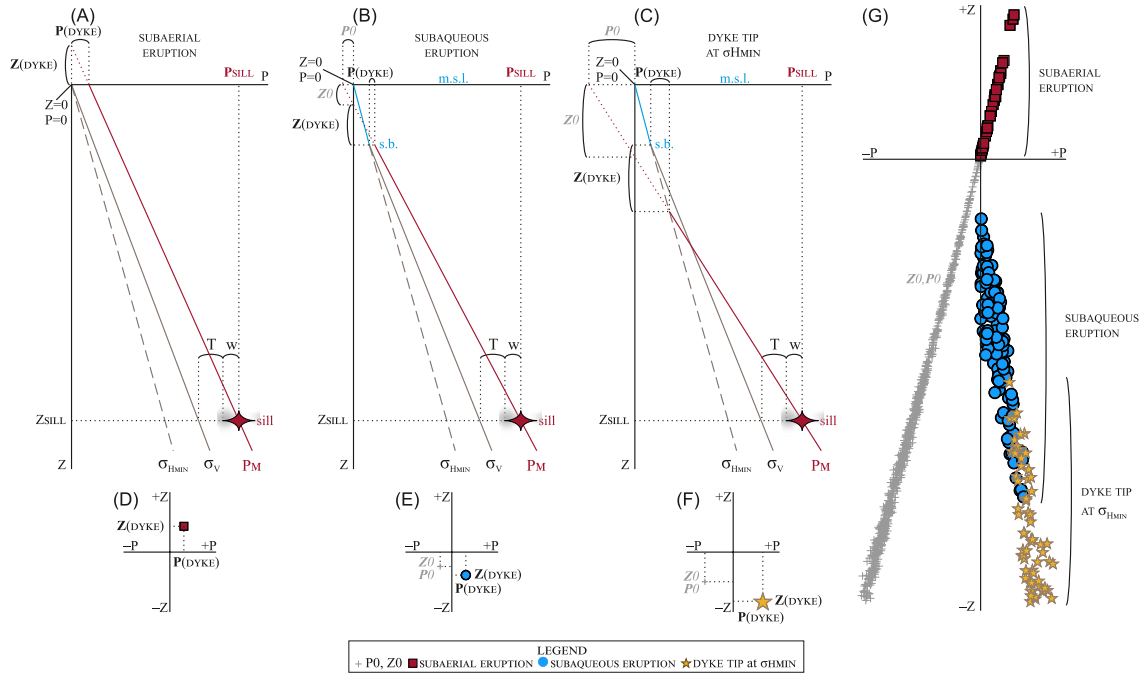

Figure 3. Illustrative single pressure-depth plots. (a) Vertical stress σ_V, minimum horizontal stress σ_{Hmin}, and magma pressure P_M anchored at P_{SILL} (see Equation 3). P_M intersects the surface ($Z = 0$) with pressure $P_{\mathrm{DYKE}} > 0$ resulting in a subaerial expulsion of magma, $Z_{\mathrm{DYKE}} > 0$. (b) Vertical stress σ_V, minimum horizontal stress σ_{Hmin}, and magma pressure P_M anchored at P_{SILL} (see Equation 3). P_M intersects the water column resulting in a subaqueous eruption, with $P_{\mathrm{DYKE}} > 0$ with respect to σ_V calculated at the seabed (s.b.) and $Z_{\mathrm{DYKE}} < 0$. The projection of P_M to the surface results in the parameter $P0 < 0$ and $Z0 < 0$. (c) Vertical stress σ_V, minimum horizontal stress σ_{Hmin}, and magma pressure P_M anchored at P_{SILL} (see Equation 3). P_M intersects σ_{Hmin} below seabed surface resulting into an arrest of the dyke tip. $P_{\mathrm{DYKE}} > 0$ with respect to σ_V is calculated at the seabed (s.b.) and $Z_{\mathrm{DYKE}} < 0$. (d) Scatter plot of P_{DYKE} versus Z_{DYKE} from (a). (e) Scatter plot of P_{DYKE} versus Z_{DYKE} and $P0$ versus $Z0$ from (b). (f) Scatter plot of P_{DYKE} versus Z_{DYKE} and $P0$ versus $Z0$ from (c). (g) Illustrative scatter plot showing a distribution of P_{DYKE} versus Z_{DYKE} and $P0$ versus $Z0$ based on scatter plots shown in (d)–(f).

(Figure 3d). The second example (Figure 3b) shows a case in a shallow marine basinal setting where a sill at the same depth Z and values for T and w as in Figure 3a but with a mid-range magma density results in a subaqueous eruption because the upward extrapolation of the magma pressure upwards within the dyke is projected to intersect the selected value of the σ_{min} gradient above the sediment/water interface (Figure 3e). The final example shows a sill at the same depth Z and values for T and w as in Figure 3a but with the maximum magma density giving a magma pressure gradient that results in an intersection with the same σ_{min} gradient as in Figure 3b at a depth Z_d below the sediment/water interface (Figure 3f).

These three examples are three out of the $1{\cdot}10^6$ iterations of magma pressure and pressure-depth relationships generated within the Monte Carlo framework. Figure 3g shows a larger sample of intersection points (equivalent to those shown in Figures 3d–3f) from the full suite of iterations for one locality. This gives a sense of the range of possible outcomes for the full span of the ranges in unit boundary depths, sill depth, rock unit and magma densities and σ_{min} gradients. The Monte Carlo simulations thus provide a basis for assessing the probability of surface eruption or subsurface depth of the upper tip position of a feeder dyke to any sill.

3. Results

We reconstructed the magma pressure with depth for six locations (Stations 1–6) in total along the traverse of the Mull Dyke Swarm (Figure 1). Of these, Stations 1 and 2 are associated with the Blyth Group of dykes, and Stations 3–5 with the Cleveland Dyke (Carver et al., 2023; MacDonald et al., 1988). Station 6 was chosen to provide a reference magma pressure baseline for the pressure closer to the source on Mull from which to compare the pressure distribution in the more distal localities. Station 1 is described in detail below to illustrate our approach to reconstruction and to outline the major uncertainties in the key parameters. Geological information used in the pressure reconstructions for the other 5 stations is included in Supporting Information S1.

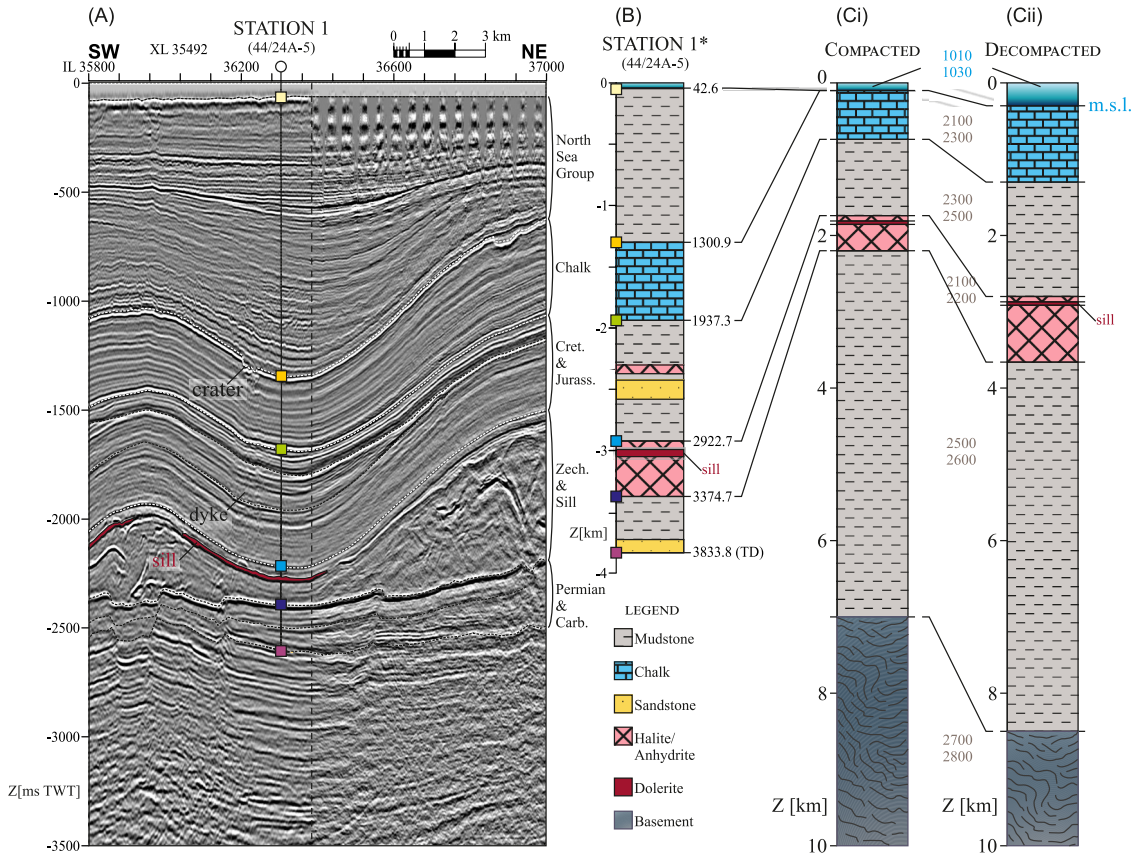

Figure 4. Geological context for Station 1 from seismic and borehole data. (a) SW-NE seismic cross section intersecting the southern proportion of the Dogger Sill Complex (sill) showing main lithological units, the sill, the crater associated to the dyke, and location of the well 44/24A-5. IL = inline; XL = crosslines. (b) Stratigraphic column from well 44/24A-5. (c) Two reconstructed stratigraphic columns for Station 1 with compacted (Ci) and fully decompacted (Cii) cases with density ranges in kg·m^{-3}.

3.1. Detailed Description and Analysis of Station 1: Well 44/24a-5 Dogger Sill Complex

3.1.1. Input Parameters From the Geology

Station 1 is the most distal of the six stations for which we reconstruct the magma pressure. It is located within the SPB in the North Sea at the position of exploration well 44/24a-5 (Figures 1 and 4). The well was drilled on the flanks of a major fold in the post-Permian overburden, and 2.3 km to the NE of the nearest mapped dyke (Figure 4a). The well intersected a 47 m thick sill intruded into evaporite rocks of the Zechstein Group at a present-day depth of 3,028 m (Figure 4b). The intersected sill forms part of the Dogger Sill Complex, which covers an area of 429 Km^2 with a total intruded volume of ~22 km^3 (Figure 1) (Cartwright et al., 2025).

The well location is close to the axis of Cenozoic subsidence in the southern North Sea hence reconstruction of the sill depth emplacement depth requires decompaction of the overburden up to and including the Late Paleocene stratigraphy. There is no evidence of any erosion within the Cenozoic at this station, hence no correction needs to be applied to replace any eroded unit thicknesses.

A reconstruction of the 1-D geology in a 10 km column at the well location is shown in Figure 4c for the undecompacted (Ci) and compacted (Cii) thickness values of the main stratigraphic units, respectively. The range in water depth values for the Late Paleocene is taken as 100–300 m based on paleobathymetric inferences made from micropalaeontological assemblages of this stratigraphic interval (Cameron et al., 1992; Lott & Knox, 1994). Assessment of standard compaction curves for the dominant lithologies comprising the overburden yielded a thickness range of 640–1,000 m to the Chalk Group and 1,000–1,500 m to the Triassic to Lower Cretaceous interval. These values reflect the probable range of decompacted thickness values taking into account uncertainties in porosity versus effective stress plots (see Text S1 in Supporting Information S1). The thickness

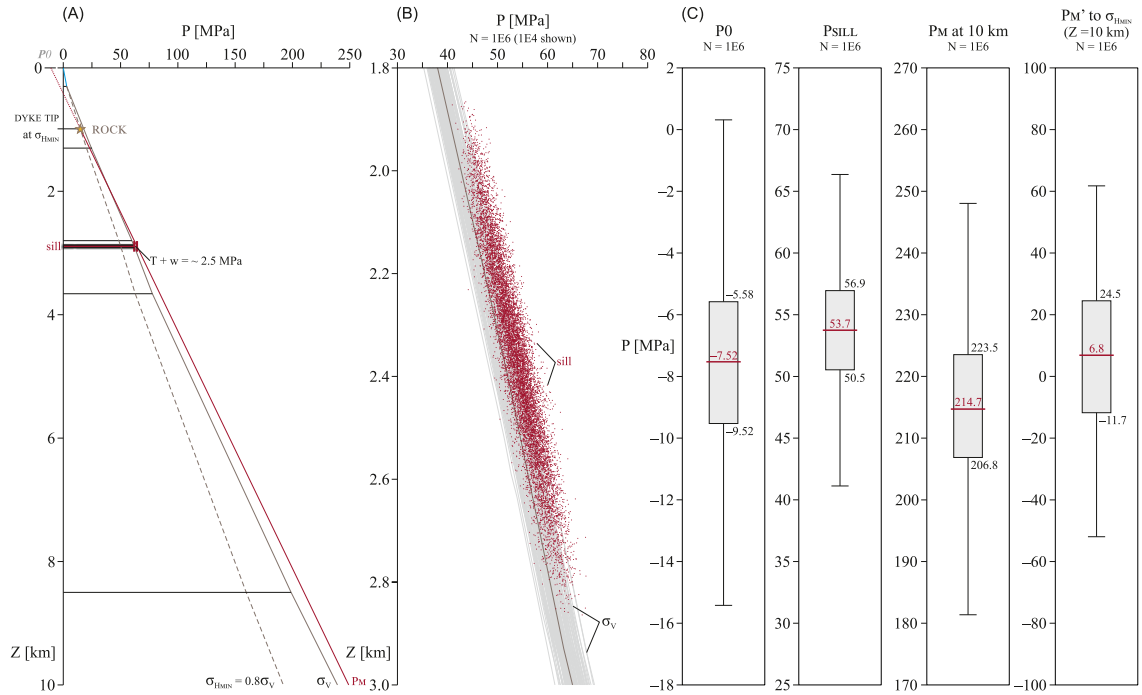

Figure 5. Pressure depth reconstruction of Station 1. (a) Pressure depth plot with vertical stress σ_V, minimum horizontal stress σ_{Hmin}, and magma pressure P_M anchored at P_{SILL} (see Equation 3). (b), subsampled scatter plot of $1{\cdot}10^4$ sill depth-pressure pairs, and $1{\cdot}10^4$ σ_V. (c) Boxplots of $1{\cdot}10^6$ iterations for $P0$, P_{SILL}, P_M at 10 km and effective magma pressure $P_M{'}$ at σ_{Hmin} at 10 km (c). Shown P25, median, and P75 values in MPa.

range of 460–860 m was assigned for the Zechstein Group to adjust for the possible magnitude of halite flow into the nearby salt cored anticlines after emplacement of the sill at c. 58 Ma (Hughes & Davison, 1993; Stewart & Coward, 1995). The two stratigraphic columns shown in Figure 4 represent the upper and lower bound cases for sedimentary unit thicknesses and rock densities. Where the present-day thicknesses are decompacted to the maximum value at the time of sill intrusion (Cii), the sill depth is c. 1,000 m deeper and the top of the crystalline basement is 1,500 m deeper than for the undecompacted case (Ci).

The well terminated in Upper Carboniferous shales at a depth of 3,874 m (Table 2). Lower Permian and Carboniferous thickness values are taken from the well data, depth conversion of the seismic data, and from gravity modeling (Fairhead et al., 2023; Kimbell & Williamson, 2015). The crystalline basement is assigned to low grade metasediments of the Avalonia Microplate based on regional modeling of gravity and magnetic data along with interpretation of deep reflection and wide-angle seismic data (Beamish et al., 2016; Pharaoh, 1999).

3.1.2. Pressure Reconstructions

The reconstruction of pressure conditions necessary to form the sill intersected in 44/24a-5 are shown in Figure 5. To illustrate the approach taken, a single reconstruction is shown in which the maximum decompacted thicknesses (Figure 4Cii) are used to reconstruct the depth of the sill at 58 Ma BP (Figure 5a). Using the maximum water depth of 300 m, the reconstructed sill depth is 2,920 m. Taking the maximum of the range of values for tensile strength of the evaporite host rocks (2 MPa) and the pressure corresponding to the work done to inflate a 47 m thick sill (0.5 MPa), the magma pressure required to form this sill (P_{SILL}) is 60 MPa. Upward projection of this value using a static gradient of 26.0 MPa·km^{-1} (mid case magma density of 2,650 kg·m^{-3}) shows that the magma pressure gradient line would intersect the gradient of $0.8{\cdot}\sigma_V$ at 1,400 m below sea level. This implies that for this single set of parameters we could expect to see the upper dyke tip at 1,100 m below the seafloor.

The results of the $1{\cdot}10^6$ Monte Carlo simulations are shown in Figure 5b with the scatter plot showing the simulated magma pressure distribution for the full range in all the input parameters. The plot shows a dominant clustering of sill magma pressure (P_{SILL}) between 48 and 63 MPa spread over a large range (c. 750 m) of depth (Z)

values. When the full range in P_{SILL} and Z is extrapolated up to the surface, it results in a scatter of values for excess pressure at surface ranging from −15.3 to 0.3 MPa (Figure 5c).

The downward extrapolation of P_{SILL} to the 10 km reference depth resulted in a much larger scatter in the simulations (P_M ranging from 180 to 250 MPa, with P25 and P75 ranging from 206 to 223 MPa, respectively) than for the surface datum simply because the projection is over a larger vertical distance (Figure 5c). The excess pressure, P_M' at 10 km is defined by subtracting the range of σ_{Hmin} values from the Monte Carlo distribution of P_M resulting from the downward projected magma pressure values constrained at the sill intrusion. This exhibits a large range of −50 to 60 MPa, but the P25–P75 range is −11–24 MPa with a median value of c. 7 MPa. Negative values of this P_M' imply that a dyke would not form at this 10 km depth. It should be recalled that use of the static magma pressure gradients for the projections is conservative, so the negative values are probably indicative of the underestimation of magma pressure at 10 km resulting from use of the static gradient combined with the neglect of communication with any excess pressure at the source. This point is addressed further in the Discussion.

3.2. Monte Carlo Results for Station 2 to 6

Magma pressure reconstructions were undertaken for the remaining five stations using parameters derived specific to each location (Table 2). Geological context for these five stations is described briefly below. Additional details are given in Supporting Information S1. Each location has specific uncertainties due to the geological context and the quality of the background data needed to constrain individual parameters.

3.2.1. Geological Context

3.2.1.1. Station 2

The pressure reconstruction for Station 2 is based on drilling results of exploration well 44/11-3 which penetrated the most proximal (to Mull) of the constituent sills of the Dogger Sill Complex, and at 98 m, the thickest (Table 2) (Text S1 in Supporting Information S1). Located closer to the basin margin than 44/24a-5, this well location has a thinner Cenozoic cover, with the result that uncertainty in decompaction is much less. The intersected sill is fed from Dyke B of the Blyth Dyke Group (Figure 1).

3.2.1.2. Station 3

Station 3 is located at the outcrop position of a small laccolithic sill fed from the Cleveland Dyke as it transects Upper Carboniferous clastic succession within the Stainmore Trough, County Durham (Figure 1, Text S1 in Supporting Information S1) (Mills et al., 1976). It is located 328 km from the Mull Center and hence represents an almost midway position in the full trajectory of the MDS. The sill outcrops at the surface in an area where much of the post-Carboniferous cover has been eroded which means that the major uncertainty in pressure reconstruction stems from the lack of preserved overburden (Green et al., 2012). However, nearby coal exploration boreholes provide additional constraints to the stratigraphic data obtained by the British Geological Survey during regional mapping (Land, 1987; Mills et al., 1976), and allow reasonable back-projection of the eroded units to the sill location. The area was not subject to subsidence during the Cenozoic, so decompaction of projected overburden units is incorporated into the gross uncertainty ranges for projected thicknesses (Table 2).

Observations of the Cleveland Dyke within coal mines from the Durham Coalfield indicate that the dyke did not propagate upwards into the Permian Magnesian Limestone (Mills et al., 1976). There are no reports along the c. 20 km outcrop width of this unit for any contact between limestone and dolerite linked to the Cleveland Dyke. However, 10 km east of this outcrop, the dyke reappears as it transects Triassic and Jurassic strata climbing upwards through stratigraphy by over 1,000 m (Fox-Strangeways, 1992; Land, 1987). These contextual observations point to the upwards termination of the Cleveland Dyke locally due to encountering the mechanically strong 300 m thick layer of Permian limestones rather than through loss of critical magma pressure necessary to sustain upwards propagation.

3.2.1.3. Station 4

Station 4 is located 135 km from the Mull center within the outcrop area of the Prestwick-Mauchline Sill Complex. This laterally extensive sill complex covers an area of 220 km^2 and was intruded into the Permo-Carboniferous clastic sediments and interbedded lavas of the Midland Valley Graben, close to the coastline of

Ayrshire in southern Scotland (Figure 1 and Text S1 in Supporting Information S1) (Cameron & Stephenson, 1985). The dolerite sills were fed directly from the Cleveland Dyke (locally named the Stevenston-Coylton Dyke by MacGregor, 1930) and are up to 60 m thick at outcrop and in boreholes across the Ayrshire Coalfield (Eyles et al., 1949; Mykura et al., 1967). At least two major transgressive sheet intrusions are interpreted from borehole data, intruding over a stratigraphic thickness range of 1,400 m from the deepest in the Middle Coal Measures (Late Carboniferous) to the shallowest in the Mauchline Sandstone (Permian). Station 4 is located specifically to sample the shallowest of the sills to provide a narrower extrapolation to the surface in the overall pressure distributions.

The likely overburden at the time of intrusion consisted of an unknown thickness of Permo-Triassic clastic sediments. Lateral projection from preserved remnants of this basin fill gives a probable thickness distribution for this overburden of 500–1,000 m (see Text S1 in Supporting Information S1). Limited additional constraint is given by the elevated ranks of the coals in the area, implying considerable maximum paleo-depth of perhaps >1,000 m. The large ranges of overburden thickness thus reflect these uncertainties in projection and restoration of overburden.

3.2.1.4. Station 5

Station 5 is located 95 km from the Mull center (Figure 1) within the outcrop area of the Bute Composite Sill (Smellie, 1915) dated as 56.3 ± 1 Ma using the K/Ar method (Buist et al., 1979). The sill is a maximum of 25 m thick and its outcrop extends for c. 2 km on the southern tip of Bute, Argyll. It was intruded into the heavily faulted lavas of the Clyde Group of the Midland Valley Graben (Early Carboniferous, Cameron & Stephenson, 1985) (Figure 1 and Text S1 in Supporting Information S1). The outcropping sill is close to the projected trajectory of the Stevenston-Coylton (Cleveland) Dyke.

The likely overburden at the time of intrusion consisted of Permo-Triassic clastic sediments deposited within the North Arran Trough and was in the range 500–1,000 m based on cross-sections of the offshore area of the Clyde region in Evans (1985). Lateral projection from preserved remnants of this basin fill across several large faults of unknown kinematic history introduces this factor of two uncertainty (see Text S1 in Supporting Information S1).

3.2.1.5. Station 6

The final station is located a few kilometers north of Loch Scammadale, c. 30 km from the center of Mull, and within the center of the main swarm of dykes as mapped by the British Geological Survey (Bailey, 1924; Kynaston & Hill, 1908). WNW trending dykes are exposed across elevation ranges of several hundred meters within a region dominated by outcropping schists of the Dalradian Supergroup (see Text S1 in Supporting Information S1). Some of these dykes have been interpreted as tipping out upwards toward the summits of the hills where outcropping dykes disappear beneath Dalradian metasediments at higher elevations along strike (Kynaston & Hill, 1908).

No sills have been identified in this area, so the pressure reconstruction was solely based on the dyke propagation criterion and using the same range of σ_{Hmin} values as deployed for the basement rocks of the Stations 4 and 5.

3.2.2. Sill Magma Pressure

The magma pressure required to form the sills (P_{SILL}) for Stations 1–5 is shown in Figure 6. A reconstruction of the notional magma pressure range at 1 km depth beneath the surface is shown for Station 6 where no sill has been reported. This pressure reconstruction is instead based on setting the Monte Carlo simulation to run with the constraint that the magma pressure at 10 km matches the range in σ_V and projecting the magma pressure gradient range upwards from this intersection. It is important to re-emphasize that these ranges for P_{SILL} are conservative and the minimum required and are not meant to imply that the actual magma pressure was restricted to these values.

The box plots in Figure 6a show that the six stations fall into two groups: the most proximal three having median values in the 20–30 MPa range, whereas the three distal stations range from 54 to 62 MPa. It should be recalled that these six stations sample the pressure in two different sub-swarms of the MDS. All six stations exhibit a relatively constrained variability in P25-P75, which is in the order of ±2.5 MPa (Figure 6a). These ranges are

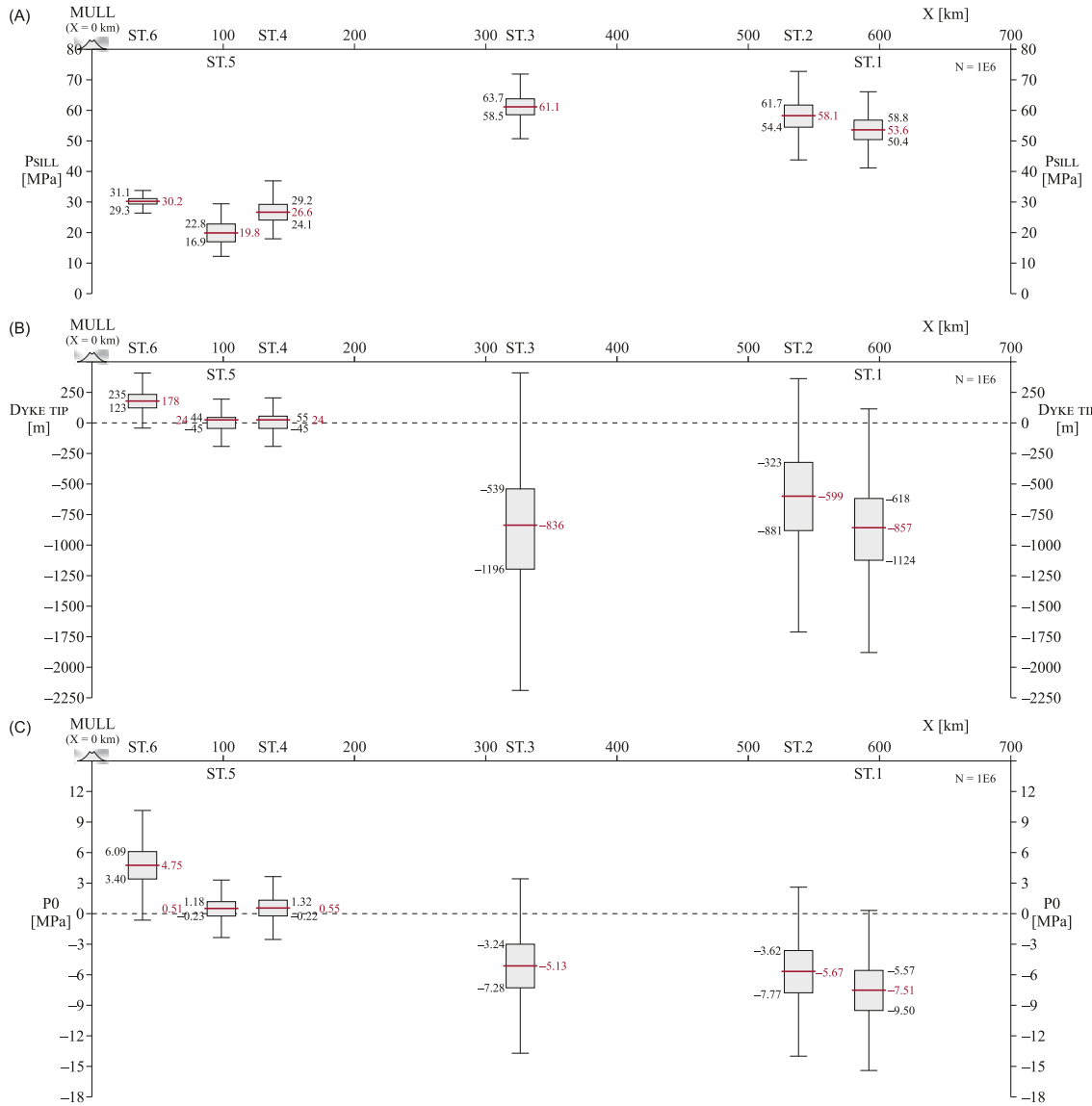

Figure 6. Boxplot sets ($N = 1{\cdot}10^6$) for Stations 1–6 over distance (relative to the Mull Volcanic Center, $X = 0$ km). Of (a) magma pressure P_{SILL} with shown P25, median, and P75 values in MPa, (b) dyke tip depth with shown P25, median, and P75 values in m, and (c) $P0$ with shown P25, median, and P75 values in MPa.

controlled by the uncertainties in the reconstructed depths of the sills in all cases which typically exceed those related to the density profile of the overburden, the tensile strength and the work done to inflate the sills.

3.2.3. Depth to Upper Dyke Tips

The results of extrapolation to surface of the sill magma pressures computed for Stations 1–5 along with the reference range for Station 6 are shown in Figures 6b and 7. Stations 1 and 2 in the southern Permian Basin have similar distributions for the predicted depths to the upper dyke tips, with the majority of data points indicating that the dykes would tip out upwards somewhere in the 500–1,500 m depth range. The median value for Station 1 is deeper at c. 860 m than that for Station 2 (c. 600 m) (Figure 6b). Only a small minority of points at the far end of the ranges for both stations indicate that surface eruption would have occurred (Figures 6b and 7). Station 3 has a similar distribution to Stations 1 and 2, albeit with a larger tail population at slightly greater depths and with a higher proportion of data points indicating eruption would have occurred (Figures 6b and 7). Its median value is 836 m (Figure 6b). Stations 4–6 have much narrower ranges than the more distal stations, which reflects the simpler geology with generally higher density rock units comprising all or the bulk of the 10 km column

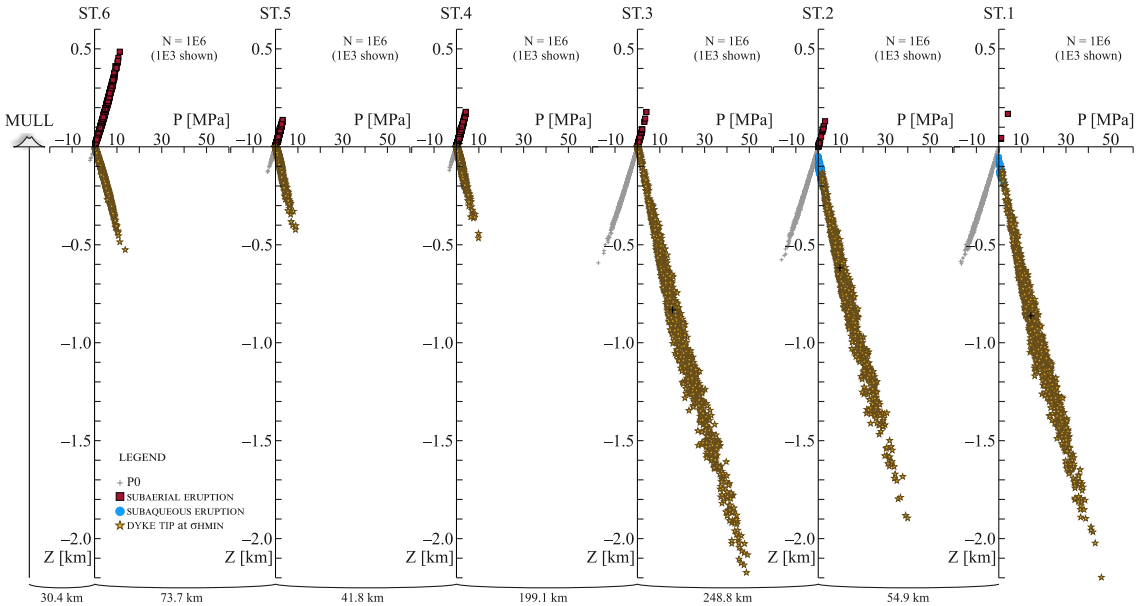

Figure 7. Scatter plot of the distribution of P_{DYKE} versus Z_{DYKE} and P_0 versus Z_0 for Stations (ST) 1 to 6 ($N = 1{\cdot}10^6$; shown $1{\cdot}10^3$) (shown as Station 1 right to Station 6 left, with inter-station distances shown). See Table 1 for notation.

(Figure 7). These three stations have distributions that straddle the surface datum (mean sea level). In all three stations the median value is positive, implying that magma pressure in the dykes was sufficient for aerial eruption to have occurred for the majority of the simulations (Figures 6b and 7).

The predicted likelihood of eruption at Stations 4–6 in the Monte Carlo simulations of depths to upper dyke tips for the six stations in our pressure reconstruction are contradicted by the evidence from the geology. There is no evidence of any extrusive igneous rocks of the same age as the dykes close to any of these three stations that would be indicative of surface eruption. At Station 3, the predicted upper tip position would be at −1,200 to −550 m whereas upper dyke tips observed in nearby coal mines would have been at depths greater than 1,500 m at the time of intrusion, which is far too deep for the most likely pressure state predicted by the conservative modeling approach. The magma pressure was almost certainly sufficient at Station 3 to achieve upward propagation of the Cleveland Dyke much closer to the contemporaneous surface. Only 30 km ESE along strike from Station 3, the Cleveland Dyke transects the Permian limestones propagating upwards to at least the level of the outcropping Middle Jurassic to a position that would have been within 500 m of the surface (see Text S1 in Supporting Information S1).

For the more distal Stations 1 and 2, the modeled upper tip positions are much deeper than the actual upper tip positions of the Blyth Dyke Group constrained from well calibration, aeromagnetic modeling and seismic interpretation. The combined geological and geophysical evidence points to the upper tips being somewhere in the range of 250–500 m beneath the sediment-water interface in the Late Paleocene (Carver et al., 2023; Pryce et al., 2025). Only those values close to the upper limit of the range match these geophysical observations.

3.3. Pressure Versus Distance From Source

The results presented in Figure 6 show that the conservatively modeled upper dyke tips consistently underestimate the likelihood of the long-range propagating dykes of the MDS reaching the surface. To place this in context, we plotted the upward extrapolated magma pressure measured at the surface datum ($Z = 0$) for each of the stations scaled with their distance from the source reservoir on Mull (Figure 6c). It should be recalled that Stations 1 and 2 are from the Blyth Group, whereas Stations 3–5 are fed by the Cleveland Dyke so co-plotting these on Figure 6c is indicative only of the pressure conditions necessary to form their respective dyke-fed sills rather than intended to show actual pressure decay trends along any single dyke.

Figure 6c shows that the magma pressure in the dykes was sufficient to ensure that they reached the surface for over 150 km from Mull and evidently failed to do so. For the first 150 km of lateral propagation, the conservative pressure reconstruction points firmly to the expectation for surface eruption (Figures 6c and 7), and for the remaining 400+ kilometers, the pressure regime in the upper tip regions was poised close to that necessary for surface eruption. For these more distal stations (1–3), any magma pressure regime that exceeded our most conservative estimation assumptions would have resulted in surface eruption as predicted for the proximal stations. If the magma pressure at the sill was only 2–4 MPa above the base line values we modeled, then the dyke pressure should have been sufficient for surface eruption along the entire length of the dykes.

In summary, the conservative modeling of the constraints provided by the geological context of the dyke-fed sills distributed over the length of the long-range lateral propagation of the MDS points decisively to a pressure state in the propagating dykes that should have led to eruption at some point in the proximal region close to the source reservoir on Mull. The explanation for why these dykes failed to erupt at any point along their 100 s of km lengths is the central question for the Discussion.

4. Discussion

4.1. The Problem of Long-Range Lateral Dyke Propagation

The most fundamental question in the genesis of giant dyke swarms such as the MDS is why they travel so far laterally from their source without erupting. The central precept for the long-range lateral propagation in giant dyke swarms is that if at any point on the lateral propagation a dyke breaches the surface, it is highly likely that flow localization would lead to lateral arrest (Ernst et al., 1995). Eruption would likely drain the magma supply to the extent that it inhibited attempts at further lateral propagation. This limiting factor was instrumental in the relatively recent fissure eruption at Holuruhan, Iceland where a c. 50 km long dyke terminated at the site of the fissure eruption (Woods et al., 2019). The flow to any eruption site would exploit the maximum pressure gradient between the injection point and the eruption site. Hence to answer why dykes propagate laterally over huge distances it is necessary to explain why they were not able to reach the surface at any point en-route.

Since the MDS is arguably one of the best documented of the many hundreds of giant dyke swarms on the terrestrial planets it is an ideal case study on which to base a discussion of why there was no eruption. The detailed mapping of dyke trajectories continuously for over 600 km (Carver et al., 2023) combined with the extensive petrological and geochemical constraints of the dykes (Macdonald et al., 1988, 2009, 2010, 2015; Ishizuka et al., 2017; Kerr et al., 1999) means that there is a foundation of basic constraints with which to discuss the wider questions. To this foundation, our identification and synthesis of dyke-fed sills along the MDS and the modeling of pressure conditions necessary to form them provides a novel analytical opportunity to address this fundamental question of the failure to erupt.

How then do these pressure reconstructions allow us to evaluate existing models for long-range lateral propagation of dyke swarms more generally, and can we use them to evaluate mechanisms that have been suggested to explain the failure for laterally propagating dykes to erupt at surface?

4.2. Possible Models for Upward Arrest During Lateral Propagation

4.2.1. Loss of Buoyancy

Most previous discussions of upward arrest below the surface focus on a mechanism that derives from the loss of buoyancy in the magma once a dyke propagates above the level of neutral buoyancy (LNB) (Chen et al., 2011; Fialko & Rubin, 1999; Lister & Kerr, 1991; Ryan, 1987; Townsend et al., 2017; Walker, 1989; Wilson & Head, 1981). The magma buoyancy is a function of the density distribution in the host rocks for the propagating dyke relative to magma density (Ryan, 1987). In this analytical framework where a dyke propagates vertically across a density stratified medium, a dyke may "overshoot" the LNB if the positive buoyancy of the deeper levels exceeds the negative buoyancy of the shallower levels but would arrest below the surface if this is not the case (Taisne & Jaupart, 2009).

A simplified cross section from the source of the dykes on Mull to the lateral tip of the longest dykes in the southern North Sea shows the gross density stratification of the host rocks and the position of the LNB for magma densities ranging from 2,550 to 2,750 km·m^{-3} (Figure 8a). This cross-section shows a large range in depth to the

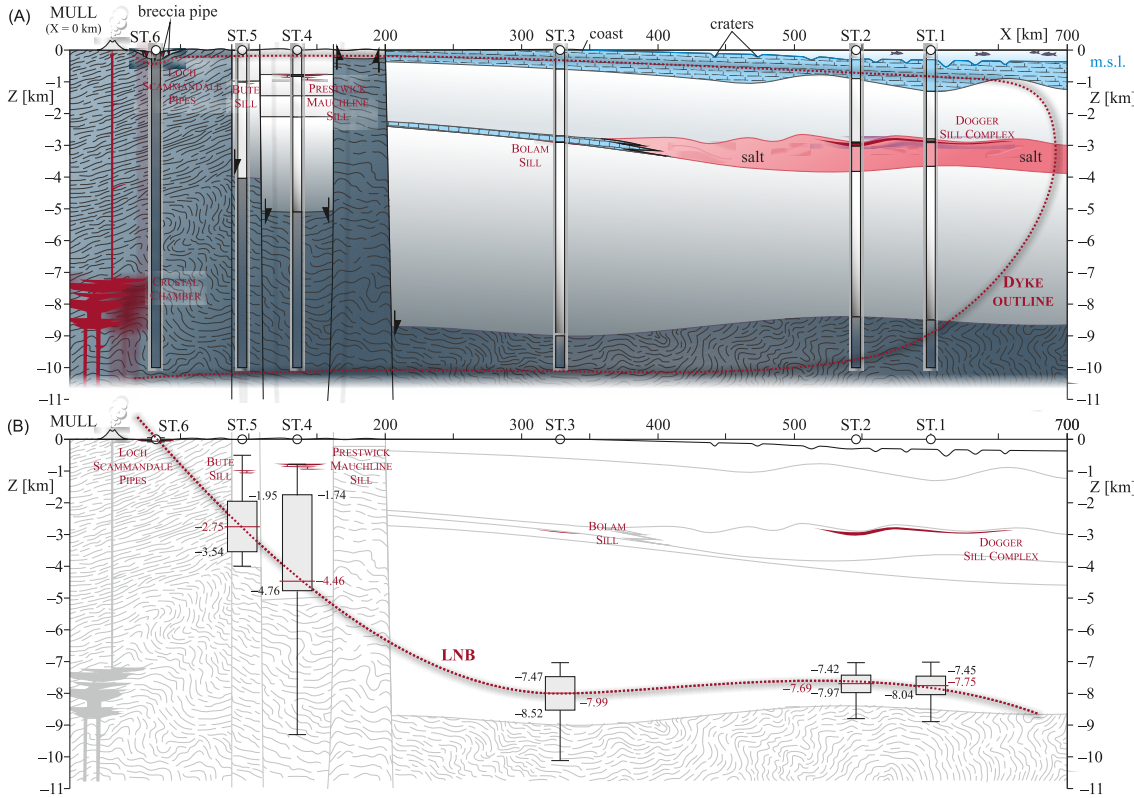

Figure 8. (a) Synoptic geological section along the general trajectory of the Mull Dyke Swarm reconstructed at 58 Ma with the main geological units, and structural elements. An outline of the dyke is shown with the tip position as the red dotted line. Also shown are the expected position and depth of the magma reservoir beneath Mull (from Ishizuka et al., 2017), and the position of Stations 1–6. (b) Boxplots showing the Monte-Carlo reconstruction of the level of neutral buoyancy (LNB) at each station.

LNB across the full length of the dyke swarm (Figure 8b). The projected magma pressure at surface derived from our Monte Carlo simulations shows that pressure was sufficient for eruption for the first 150 km of the transect (Figures 6b, 6c, and 7), and the magma was positively buoyant to the surface due to the high density of the metamorphic rocks comprising the upper crustal geology. The fact that no eruption occurred therefore implies that loss of buoyancy of the magma upwards cannot be the explanation since by a buoyancy argument alone, eruption should have occurred.

4.2.2. Mechanical or Stress Barriers

As an alternative to loss of buoyancy for the failure of the dykes to erupt, a number of theoretical, modeling and empirical studies have suggested that upward arrest is due to the dyke encountering a mechanical barrier where an overlying layer is too strong to be fractured with the available magma pressure, or where there is a discontinuity between layers of strongly contrasting properties (Gretener, 1969; Gudmundsson, 2020; Kavanagh & Sparks, 2011; Taisne & Jaupart, 2009). A variant of this mechanical mechanism is if the dyke encounters a stress barrier such as a locally enhanced horizontal compressive stress where local stress state precludes further ascent (Gudmundsson, 2020).

Upward arrest at mechanical barriers has been invoked to explain some of the gaps in the outcrop patterns of individual dykes of the Mull Dyke Swarm, as for example, with the absence of any trace of any of the dykes being observed across the outcrop of the Permian Limestone of NE England (Land, 1974). Other notable gaps occur in NW England and Southern Scotland where it seems probable that the upper tips are concealed at depth (Busby et al., 2009; Cameron & Stephenson, 1985; Dagley et al., 2008). Additionally, upper tips have also been inferred nearer to Mull, where dykes hosted in outcropping Dalradian schists disappear laterally beneath a cover of Dalradian quartzites (Kynaston & Hill, 1908). However, this explanation is extremely unlikely to apply uniformly along the dyke transect because the dykes are continuous across many areas where the host rocks contain a large

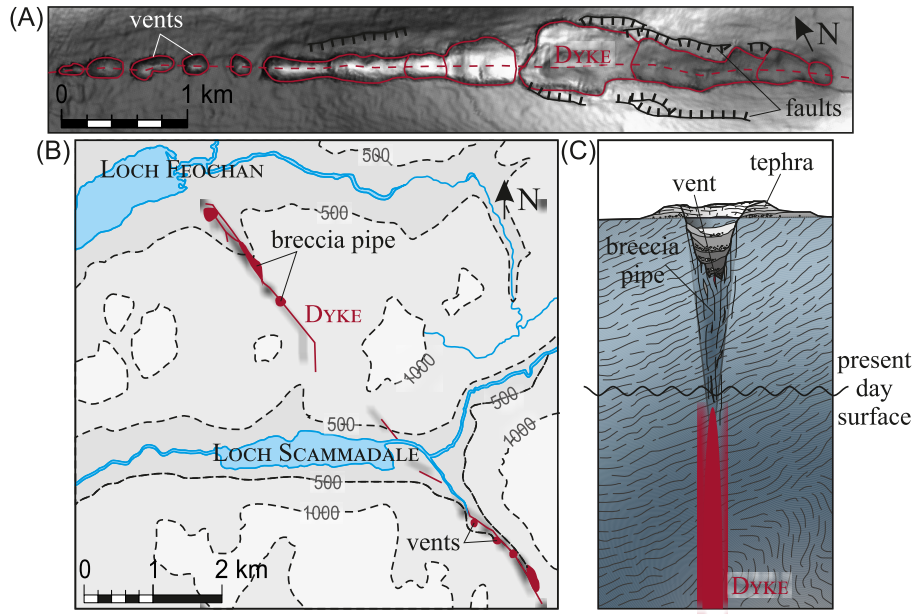

Figure 9. (a) Map of Top Cretaceous showing a linear chain of craters above the upper tip of one of the Blyth sub-swarm of dykes from the southern North Sea. This chain of craters extends for >200 km along the strike of the sub-swarm (Pryce et al., 2025). (b) Geological map showing breccia pipes associated with dykes of the MDS near Loch Scammadale (Station 6, see Figure 1) (from Bailey, 1924, p. 364; Kynaston & Hill, 1908, p. 135). (c) Reconstruction of the breccia pipe in Loch Scammadale at the time of dyke intrusion showing the interpreted vent and tephra (now eroded).

range of lithologies with highly contrasting mechanical properties (Figure 8). Furthermore, for the most distal 250 km of the Blyth Group, the upper tips of the dykes are embedded within a single lithology, the porous carbonates of the Chalk Group (Carver et al., 2023) where there is no obvious mechanical contrast that could explain their specific tip position. We acknowledge that there are uncertainties in the upper tip geometries and in the direction of magma flow toward the near surface. These uncertainties may in future be resolved by studies of anisotropic magnetic susceptibility (AMS).

4.2.3. Thermal Barriers

Relatively modest reductions in temperature of magma are known to result in large increases in magma viscosity. For example, only modest temperature reduction of 100–200°C results in three to six orders of magnitude increase in viscosity for magma of basaltic composition (Delaney & Pollard, 1982; Spera, 2000). Since magma flow velocity in a dyke is inversely proportional to magma viscosity (Gonnermann & Taisne, 2015; Lister & Kerr, 1991; Rubin, 1995), any cooling would lead to reduction in propagation velocity since the tip velocity is regulated by the ability of magma to flow into the tip region through a section of the dyke where aperture (dyke width) is decreasing. This combination of cooling and aperture reduction can therefore lead to the upward stalling of dykes. Such a thermal barrier mechanism has been invoked previously to explain the limits to lateral propagation (Delaney & Pollard, 1982; Fialko & Rubin, 1999; Lister & Kerr, 1991; Rubin, 1995).

A specific form of thermal barrier mechanism has been invoked in recent analyses of the long-range propagation of the MDS. It has been proposed that the upward arrest of dykes within the MDS is primarily due to near surface groundwater interactions leading to rapid cooling of dyke magma (Carver et al., 2023; Pryce et al., 2025). These authors envisaged that the reduction in propagation velocity with increased viscosity would increase the time for groundwater interaction with the magma possibly leading to convective as well as conductive heat transfer at the dyke walls and the development of a positive feedback loop. Delaney (1982) modeled the heat transfer as the system evolves from thermal pressurization flow of the groundwater away from the contact zone to longer term buoyancy flow in which groundwater is drawn in toward the contact and upwards toward the surface.

Recent discovery of a tephra apron and tuff deposits associated with chains of craters above the upper tips of the Blyth Group of dykes in the southern Permian Basin (Figure 9a) has provided key evidence for the

phreatomagmatic nature of the craters (Pryce et al., 2025), and hence demonstrates the critical role played by groundwater-magma interaction along a c. 200 km sector of the distal sector of the MDS. More generally, in other laterally propagating dykes on Earth, groundwater could be expected to play such a critical role wherever the near surface geology comprises porous sedimentary or volcanoclastic units. It might be less expected in areas of near surface crystalline rocks.

Surprisingly then, nearer to the source on Mull, linear zones of brecciated country rocks were reported in the earliest mapping of the MDS on the Scottish mainland, some 20–30 km SE of Mull. These breccia zones align along the trajectory of several of the larger dykes emanating from the Mull Center (Figure 9b) (Bailey, 1924, p. 364; Kynaston & Hill, 1908, p. 135). The breccias have been described as having matrix materials of altered basaltic composition (Kynaston & Hill, 1908). By analogy with similar agglomeratic breccia developed in conjunction with dykes elsewhere it is suggested that these linear breccias may represent the deeply eroded roots of diatremal pipes that developed by explosive interaction of dyke magma with the host groundwater (Lorenz, 1986) (Figure 9c). Since the host rocks are Dalradian metasediments, it can only be concluded that any groundwater present was in fractures rather than pore space, but this could have delivered the necessary flow to the contact zone to create the conditions needed for explosivity (Lorenz, 2003).

In summary, there is compelling evidence for near surface groundwater interactions at both ends of the dyke swarm, where the magma pressure was at its highest and lowest. Coupled with the inapplicability of either of the more classical explanations for upward dyke arrest, this evidence firmly points to groundwater interaction and cooling and the concomitant increase in magma viscosity as the dominant factor in the failure of the dykes to erupt.

4.3. Pressure Distribution Along the Dyke Trajectory and Implications for Source Pressure

What can we infer, if anything from these pressure reconstructions about the likely magnitude of the pressure in the source reservoir? The source pressure is the driver for any laterally propagating dyke, but of all the components in the magmatic plumbing system, this is the least constrained (Rubin, 1995). A lateral pressure gradient of 200 $Pa{\cdot}m^{-1}$ was estimated for laterally propagating dykes in the Rift Zones of Kilauea (Rubin & Pollard, 1987) based on a typical dyke thickness of 1 m and a magma flow velocity of 0.5 $m{\cdot}s^{-1}$. In contrast, Fialko and Rubin (1999) adopt a value of 50 $Pa{\cdot}m^{-1}$ for their calculations of dyke geometry and magma flow in laterally propagating dykes. The importance of source pressure stems from the fundamental principle that the magma pressure in the propagating dyke is entirely dependent on the source pressure at the injection point together with pressure losses during transport (Lister & Kerr, 1991; Rubin, 1995; Rubin & Pollard, 1987). To achieve long-range lateral propagation the magma pressure at any point in the actively propagating dyke must be in open pressure communication with the source pressure (Macdonald et al., 1988). Pressure communication follows from the need to secure sufficient magma flux to drive the dyke propagation laterally.

Assuming pressure communication over the full dimensions of the dyke, then the maximum lateral pressure gradient will be along a line parallel to the surface from the injection point (Figure 10). The source pressure P_M is influenced by the density structure vertically above the confined source reservoir because it is the load acting on the fluid that equates to the static pressure in the reservoir (Gudmundsson, 2020). However, the vertical load at points on a horizontal line distant from the reservoir (e.g., Xi, Xii, Xiii on Figure 11) does not pressurize the magma in the dyke. The magma pressure is "blind" to the density distribution above this line (Rubin, 1995) and is only dependent on the source (injection) pressure P_M, the lateral pressure gradient and the distance from the injection point. At any point along the lateral trajectory, the magma pressure at surface does not depend on the loss of buoyancy with height as the dyke transects rock units of lower density than the magma itself. The expected decrease in magma pressure measured at points that are increasingly further from the source is simply due to work done during dyke propagation and magma transport not due to density stratification. As depicted in Figure 10, the driver for lateral propagation is not the inclined LNB and its impact on buoyancy but the influence of the density structure on confining stress σ_{Hmin}. As convincingly argued by Buck et al. (2006), the ability of the dyke to propagate laterally is dominantly a competition between magma pressure and confining stress. Hence as pressure losses accumulate downstream, the reduction in confining stress resulting from lighter rock columns above the datum maintains the viability of dyke propagation.

To place the propagation of the MDS in the wider context of the preceding discussion, we estimated the possible range of magma pressures that could have pertained in the shallow magma chamber beneath the Mull volcano

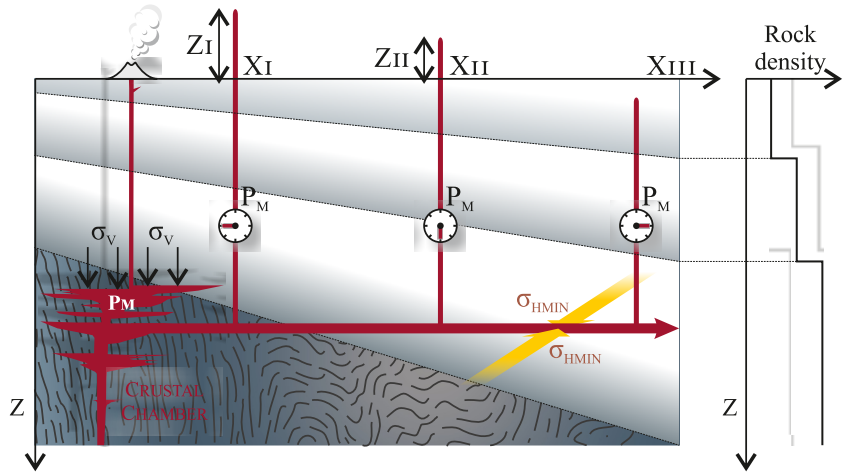

Figure 10. Conceptual cross-section showing magma pressure distribution along a laterally propagating dyke emanating from an injection point in the subvolcanic reservoir beneath Mull. The magma pressure P_M in the source reservoir is directly related to the vertical load σ_V on the magma chamber. The lateral migration of magma over distance is controlled by the competition of the magma pressure and the confining stress (σ_{Hmin}) acting on the wall of the dyke. At locations X_I to X_{III} the magma pressure within the dyke P_M decreases due to viscous losses but not due to the lateral variation in overburden density (symbolized by the height of the thick red vertical lines). This results in a lower likelihood of subaerial eruption distally from the injection point.

prior to the lateral injection into the dyke swarm. Subsurface constraints on the crustal structure beneath Mull are limited to interpretation of a large negative bouguer gravity anomaly (c. 80 mGals) centered on Mull and believed to represent the solidified accumulation of the sub-volcanic magma reservoirs that fed the volcano and the MDS during the c. 3 million years of activity of the Mull center (Bott & Tantrigoda, 1987).

Using the crustal model from Bott and Tantrigoda (1987) and their best fit values for the density of the major rock units in the crust as input, we performed a set of Monte Carlo simulations ($N = 1{\cdot}10^6$) using the error ranges in depth and density adopted in their gravity inversion to compute the range in magma pressure values in the source reservoir for a chamber depth at 10 km (Text S1 in Supporting Information S1). This distribution is tightly clustered with a median value of 313 MPa and a P25 to P75 range of 309 and 317 MPa, respectively (Figure 11). This magma pressure was obtained by making the simple conservative assumption that the magma pressure in the magma chamber must be at least equal to the overburden load (σ_V). This assumption matches criteria for failure at the margins of a sill-like magma chamber (Buck et al., 2006; McLeod & Tait, 1999; Rivalta, 2010) but being conservative neglects any excess pressure above this minimum that could be contributed by communication with

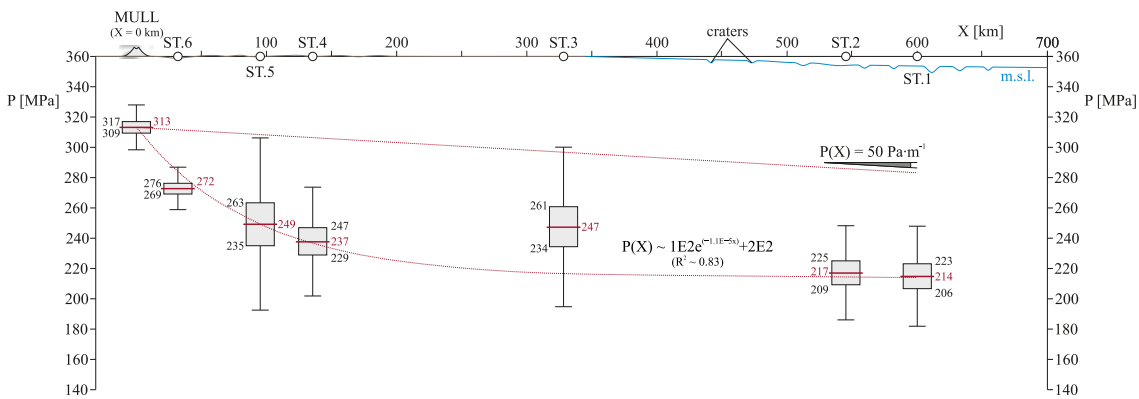

Figure 11. Vertical total stress reconstruction at the Mull Volcanic Center (MVC; $X = 0$ km) and magma pressure reconstruction at a depth of 10 km from Station 1–6 against distance. A linear pressure decay of 50 Pa·m^{-1} would overestimate the pressure along the entire dyke. Conversely, an exponential fitting curve shows a good approximation ($R^2 \sim 0.83$) of pressure decay away from the MVC, although we emphasize this plot groups together stations that represent different dykes within the MDS. Therefore, this best fit curve is only indicative of the possible pressure reduction with distance.

a deeper magma source, or from for example, magma chamber dynamics (e.g., fractional crystallization, exsolution; Rivalta, 2010).

We plotted the computed distribution for the magma chamber pressure beneath Mull against the Monte Carlo distribution of magma pressure at 10 km depth reconstructed for Stations 1–6 scaled for distance (Figure 11). For Stations 1–5, the magma pressure at 10 km was obtained by extrapolating downwards from the constraints afforded by the sills. For Station 6, the pressure at 10 km was simply equated to the Monte Carlo distribution of σ_V.

The resulting plot in Figure 11 should be viewed as only indicative of pressure versus distance since we are grouping stations from different sub-swarms. At face value therefore, this could be taken as showing a crudely exponential decrease in pressure with distance from the source. However, the ranges in pressure for individual stations are such that a linear trend could also be fitted if the pressure in the sub-volcanic chamber was lower by 15–20 MPa. This lower pressure in the chamber is certainly feasible if only a fraction of the sub-volcanic mass anomaly was in place by the time the major dykes were intruded.

Magma pressure gradients for laterally propagating dykes are commonly assumed as linear in a horizontal direction in theoretical treatments of dyke emplacement and typically estimated from considerations of magma source pressure and realistic stress intensity factors needed to maintain propagation in upper crustal rocks. We co-plotted the 50 $Pa{\cdot}m^{-1}$ gradient cited by Fialko and Rubin (1999) on the Monte Carlo distributions of Figure 11 purely for comparison, and it is evident that this linear gradient value does not match the distributions from the reconstructions. It is interesting to note that if the pressure at the source is a reasonable estimate, the predicted pressure at 10 km depth for the most distal Station 1 using this 50 $Pa{\cdot}m^{-1}$ gradient would be about 70 MPa above what we conservatively estimate which in turn would imply an excess pressure at the surface of >20 MPa. Even if magma pressure decreased along a linear gradient twice that suggested by Fialko and Rubin (1999) as being a reasonable estimate for lateral propagation, excess pressure at the surface would be large enough to guarantee eruption.

The compilation of modeled pressure distributions in Figure 11 is only a crude representation but is nonetheless informative. Because it is based on conservative assumptions and importantly is grounded on the invaluable constraints provided by the conditions needed for sill formation, it is possible to argue that the magma pressure in the major dykes emanating from the source reservoir beneath Mull exceeded that necessary to guarantee surface eruption. This surfeit of excess pressure in the near surface means that all mechanisms reliant on loss of pressure to explain the long-range lateral propagation cannot be applicable, and that a thermal barrier represents a viable alternative.

In conclusion, a thermal barrier to surface eruption best explains all the observations and modeled pressure reconstructions for the MDS and will be more widely applicable to other giant dyke swarms, particularly those on Earth. All that is required is a sufficiently efficient cooling mechanism in the near surface to overcome the potential energy release available in excess magma pressure. Such conditions are likely wherever there is high thermal conductivity in the near surface host rocks, or the potential for heat loss through convection, advection or phase changes in near surface materials.

4.4. Limitations to Our Reconstructed Pressure Distributions

Our pressure reconstructions were based on five data points where we were confident that the pressure could be constrained by the sill intrusions. There may well be additional sills present along the 650 km strike length of the MDS, but these have not been reported in the literature. The large gaps between stations introduces some inevitable spatial uncertainty, for example, in the assessment of the lateral pressure decline (Figure 11). To compensate for the small number of stations we grouped the two sub-swarms together to gain a gross view of the pressure variations laterally. These two sub-swarms almost certainly formed at slightly different times (Carver et al., 2023) and with likely different injection pressures in the source reservoir and contrasting pressure decay characteristics. Hence, our grouped distributions should be taken only as indicative, enabling a crude comparison to theoretical lateral pressure gradients. By constructing this indicative plot (Figure 11) we aim to focus attention on the wider need to better constrain lateral pressure decay in laterally propagating dykes.

We have followed previous work in using static pressure gradients acknowledging that our conservative estimates are best served by using a static gradient. Our conservative approach does not therefore reproduce the actual

pressures during propagation, but only the minimum required to form the sills. Furthermore, we do not know whether the sills were intruded during the active phase of propagation as the tips advanced to the SE, or during a waning stage after the lateral limit had been reached. If the latter applied, then the estimates for pressure for sill intrusion would likely underestimate the peak pressures during the active propagation phase. This enhanced active pressure (relative to the waning pressure) would increase the likelihood of eruption en route.

We have also tacitly assumed laminar flow of the magma in our discussion, whereas Macdonald et al. (1988) make a persuasive case for the possibility of transitional flow behavior between laminar and turbulent. They drew attention to the consequences of this transitional regime for heat generation and transfer. Our observed upward narrowing of dykes toward the tips (Cartwright et al., 2025) perhaps favors laminar flow in the uppermost kilometer or so, but this needs a full quantitative evaluation.

In our study we propose a qualitative argument for the thermal barrier to upward propagation rooted in the observations of phreatomagmatic craters and the shallow depth to the upper tips of the major dykes. To quantify the cooling involved in the upwards propagation component and the consequent change in viscosity and magma flow velocity is beyond the scope of our study. This complex coupled problem of thermal transfer (via conduction, phase change, advection, and convection), fluid dynamics and deformation (such as fracturing induced by dyke dilation) does not have any current theoretical foundation, but should be a priority for future theoretical studies.

Finally, we should stress that this analysis and the suggested model of a thermal barrier are not intended to explain all lateral dyke propagation. The model is unlikely to apply where sufficient cooling in contact with host rocks cannot produce the requisite increase in viscosity. However, we believe this mechanism has been underestimated and may be more widely applicable than just the case of the MDS, particularly on Earth where dykes transect basins containing high porosity sedimentary fills.

5. Conclusions

We addressed one of the outstanding questions concerning the genesis of giant radial dyke swarms namely why the dykes fail to erupt during their long-range lateral propagation. We reconstructed the magma pressure distribution in constituent dykes of the Mull Dyke Swarm using constraints drawn from geological observations of shallow level sills that were emplaced at intervals along the >600 km strike length of the major dykes.

We simulated the magma pressure with a Monte Carlo approach based on the standard rock mechanical conditions for sill and dyke emplacement. We found that for realistic ranges of all the key parameters of magma density, host rock density, reconstructed depths to the sills and of rock unit boundaries, the dykes would have had high enough magma pressure at the sill depths to ensure surface eruption. Since surface eruption would most likely have led to lateral arrest, some mechanism must have been operative to prevent the dykes reaching the contemporary surface.

Our pressure reconstructions combined with geological observations constraining actual upper tip depths show that classical explanations for upward dyke arrest based on loss of buoyancy or mechanical barriers are inapplicable for the Mull Dyke Swarm. Instead, we propose a mechanism involving a thermal barrier due to near-surface groundwater interaction is the most plausible explanation for dyke arrest whereby cooling significantly increases magma viscosity and reduces propagation velocity to the point where the dyke stalls. Field evidence of phreatomagmatic eruptions above dyke tips at both proximal and distal ends of the dyke swarm supports the role of groundwater-driven cooling in stalling the dykes.

Our pressure reconstructions provide a direct constraint on the decay of magma pressure with distance from the source reservoir. We find that this decay curve exhibits an exponential rather than linear form although we note that uncertainty in the source pressure beneath Mull should be borne in mind. The use of sills to reconstruct magma pressure in laterally propagating dykes has not been undertaken previously but has considerable potential more widely in providing much needed constraints for the range of theoretical models for long-range lateral dyke propagation.

Conflict of Interest

The authors declare no conflicts of interest relevant to this study.

Data Availability Statement

The geological framework used to reconstruct the depth of the sill intrusions at the time of the dyke swarm emplacement (58 Ma) is described in Text S1 in Supporting Information S1. The Monte Carlo method applied to estimate magma pressures is detailed in Text S2 in Supporting Information S1. All input data used in this study are available in machine-readable format and archived on Zenodo (Foschi & Cartwright, 2025a): https://doi.org/10.5281/zenodo.16752884. The MATLAB code used to implement the Monte Carlo pressure simulations is also available at Zenodo (Foschi & Cartwright, 2025b): https://doi.org/10.5281/zenodo.16752884. These resources are cited in the References section.

Acknowledgments
We thank the Editors and reviewers Richard Ernst and Lionel Wilson for their thoughtful and insightful reviews. We are grateful to Schlumberger for providing an academic license of Petrel. The paper contains information provided by the North Sea Transition Authority and/or other third parties. This research received no specific grant from any funding agency in the public, commercial or not-for-profit sectors. We thank David James for general background discussions on sill and dyke intrusions, and Richard Katz for discussions on the level of neutral buoyancy. We also thank David Pyle for discussions on magma viscosity and propagation. We thank Ben Aldridge and Daniel Philips for discussion on seismic interpretation and well database. We finally thank Nadine Appleton for helping proofread the plain text summary.

References

Ahlers, S., Henk, A., Hergert, T., Reiter, K., Müller, B., Röckel, L., et al. (2021). 3D crustal stress state of Germany according to a data-calibrated geomechanical model. *Solid Earth*, *12*(8), 1777–1799. https://doi.org/10.5194/se-12-1777-2021

Bailey, E. B. (1924). *Tertiary and post-tertiary geology of Mull, Loch Aline, and Oban: A description of parts of sheets 43, 44, 51, and 52 of the geological map* (Vol. 43). HM Stationery Office.

Bailey, E. B. (1934). West Highland tectonics: Loch Leven to Glen Roy. *Quarterly Journal of the Geological Society*, *90*(1–4), 462–525. https://doi.org/10.1144/GSL.JGS.1934.090.01-04.16

Barton, P. J. (1992). LISPB revisited: A new look under the Caledonides of northern Britain. *Geophysical Journal International*, *110*(2), 371–391. https://doi.org/10.1111/j.1365-246X.1992.tb00881.x

Beamish, D., Kimbell, G., & Pharaoh, T. (2016). The deep crustal magnetic structure of Britain. *Proceedings of the Geologists' Association*, *127*(6), 647–663. https://doi.org/10.1016/j.pgeola.2016.10.007

Behr, W. M., & Platt, J. P. (2011). A naturally constrained stress profile through the middle crust in an extensional terrane. *Earth and Planetary Science Letters*, *303*(3–4), 181–192. https://doi.org/10.1016/j.epsl.2010.11.044

Blundell, D. J. (1993). Deep structure of the Anglo–Brabant massif revealed by seismic profiling. *Geological Magazine*, *130*(5), 563–567. https://doi.org/10.1017/S0016756800020859

Bott, M. H. P., Swinburn, P. M., & Long, R. E. (1984). Deep structure and origin of the Northumberland and Stainmore troughs. *Proceedings of the Yorkshire Geological Society*, *44*(4), 479–495. https://doi.org/10.1144/pygs.44.4.479

Bott, M. H. P., & Tantrigoda, D. A. (1987). Interpretation of the gravity and magnetic anomalies over the Mull Tertiary intrusive complex, NW Scotland. *Journal of the Geological Society*, *144*(1), 17–28. https://doi.org/10.1144/gsjgs.144.1.0017

Bray, R. J., Green, P. F., & Duddy, I. R. (1992). Thermal history reconstruction using apatite fission track analysis and vitrinite reflectance: A case study from the UK East Midlands and Southern North Sea. *Geological Society, London, Special Publications*, *67*(1), 3–25. https://doi.org/10.1144/GSL.SP.1992.067.01.01

Brown, G., Platt, N. H., & McGrandle, A. (1994). The geophysical expression of Tertiary dykes in the southern North Sea. *First Break*, *12*(3), 137–146. https://doi.org/10.3997/1365-2397.1994011

Brudy, M., Zoback, M. D., Fuchs, K., Rummel, F., & Baumgärtner, J. (1997). Estimation of the complete stress tensor to 8 km depth in the KTB scientific drill holes: Implications for crustal strength. *Journal of Geophysical Research*, *102*(B8), 18453–18475. https://doi.org/10.1029/96JB02942

Buck, W. R., Einarsson, P., & Brandsdóttir, B. (2006). Tectonic stress and magma chamber size as controls on dike propagation: Constraints from the 1975–1984 Krafla rifting episode. *Journal of Geophysical Research*, *111*(B12). https://doi.org/10.1029/2005JB003879

Buist, D. S., Ineson, P. R., & Mitchell, J. G. (1979). Isotopic age determinations on the composite sill and associated olivine dolerite, South Bute. *Scottish Journal of Geology*, *15*(4), 257–262. https://doi.org/10.1144/sjg15040257

Burov, E. B., & Watts, A. B. (2006). The long-term strength of continental lithosphere: "Jelly sandwich" or "crème brûlée"? *Geological Society of America Today*, *16*(1), 4. https://doi.org/10.1130/1052-5173(2006)016<4:tltsoc>2.0.co;2

Busby, J. P., Akhurst, M. C., & Walker, A. S. D. (2009). A new high-resolution aeromagnetic dataset over central Ayrshire: Insights into the concealed geology. *Scottish Journal of Geology*, *45*(1), 1–12. https://doi.org/10.1144/0036-9276/01-370

Caldwell, W. G. E., & Young, G. M. (2013). Structural controls in the western offshore Midland Valley of Scotland: Implications for Late Palaeozoic regional tectonics. *Geological Magazine*, *150*(4), 673–698. https://doi.org/10.1017/S0016756812000878

Cameron, I. B., & Stephenson, D. (1985). *British regional geology: The Midland Valley of Scotland* (3rd ed., p. 172). British Geological Survey. London: H.M.S.O.

Cameron, T. D. J., Crosby, A., Balson, P. S., Jeffrey, D. H., Lott, G. K., Bulat, J., & Harrison, D. J. (1992). The geology of the Southern North Sea. In *United Kingdom offshore regional report*. British Geological Survey and HMSO. London.

Cartwright, J., Foschi, M., & Phillips, D. (2025). The role of sill intrusion in delimiting the lateral propagation of giant dyke swarms: Emplacement of the Dogger Sill Complex, southern North Sea. *Journal of the Geological Society*, *182*(4), jgs2025005. https://doi.org/10.1144/jgs2025-005

Carver, F., Cartwright, J., McGrandle, A., Kirkham, C., & Pryce, E. (2023). The continuation of the mull dyke swarm into the Southern North Sea. *Journal of the Geological Society*, *180*(6), jgs2023039. https://doi.org/10.1144/jgs2023-039

Chambers, L. M., & Pringle, M. S. (2001). Age and duration of activity at the Isle of Mull Tertiary igneous centre, Scotland, and confirmation of the existence of subchrons during Anomaly 26r. *Earth and Planetary Science Letters*, *193*(3–4), 333–345. https://doi.org/10.1016/S0012-821X(01)00499-X

Chen, Z., Jin, Z. H., & Johnson, S. E. (2011). Transient dike propagation and arrest near the level of neutral buoyancy. *Journal of Volcanology and Geothermal Research*, *203*(1–2), 81–86. https://doi.org/10.1016/j.jvolgeores.2011.03.005

Dagley, P., Skelhorn, R. R., Mussett, A. E., James, S., & Walsh, J. N. (2008). The Cleveland dyke in southern Scotland. *Scottish Journal of Geology*, *44*(2), 123–138. https://doi.org/10.1144/sjg44020123

Delaney, P. T. (1982). Rapid intrusion of magma into wet rock: Groundwater flow due to pore pressure increases. *Journal of Geophysical Research*, *87*(B9), 7739–7756. https://doi.org/10.1029/JB087iB09p07739

Delaney, P. T., & Pollard, D. D. (1982). Solidification of basaltic magma during flow in a dike. *American Journal of Science*, *282*(6), 856–885. https://doi.org/10.2475/ajs.282.6.856

Donato, J. A. (2020). *Gravity modelling across two postulated granite batholiths within the UK onshore East Midlands Shelf*. University of Oxford/UKOGL Beneath Britain Website.

Du Rouchet, J. D. (1981). Stress fields, a key to oil migration. *AAPG Bulletin*, *65*(1), 74–85. https://doi.org/10.1306/2F919774-16CE-11D7-8645000102C1865D

El Bilali, H., & Ernst, R. E. (2024). Far-travelled 3700 km lateral magma propagation just below the surface of Venus. *Nature Communications*, *15*(1), 1759. https://doi.org/10.1038/s41467-024-45603-6

Engelder, T., Lacazette, A., Barton, N., & Stephansson, O. (1990). Natural hydraulic fracturing. In *Proceedings of the International Symposium on Rock Joints, 4–6 June at Loen, Norway* (pp. 35–43).

England, R. W. (1988). The early Tertiary stress regime in NW Britain: Evidence from the patterns of volcanic activity. *Geological Society, London, Special Publications*, *39*(1), 381–389. https://doi.org/10.1144/GSL.SP.1988.039.01.33

England, R. W., Butler, R. W. H., & Hutton, D. H. W. (1993). The role of Paleocene magmatism in the Tertiary evolution of basins on the NW seaboard. In *Geological Society, London, petroleum geology conference series* (Vol. 4, pp. 97–105). The Geological Society of London. https://doi.org/10.1144/0040097

Ernst, R. E., Grosfils, E. B., & Mege, D. (2001). Giant dike swarms: Earth, Venus, and Mars. *Annual Review of Earth and Planetary Sciences*, *29*(1), 489–534. https://doi.org/10.1146/annurev.earth.29.1.489

Ernst, R. E., Head, J. W., Parfitt, E., Grosfils, E., & Wilson, L. (1995). Giant radiating dyke swarms on Earth and Venus. *Earth-Science Reviews*, *39*(1–2), 1–58. https://doi.org/10.1016/0012-8252(95)00017-5

Evans. (1985). *BGS 1:250,000 solid geology clyde Sheet 55N- 06W*. HMSO. London.

Evans, A. L., Fitch, F. J., & Miller, J. A. (1973). Potassium–argon age determinations on some British Tertiary igneous rocks. *Journal of the Geological Society, London*, *129*(4), 419–438. https://doi.org/10.1144/gsjgs.129.4.0419

Eyles, V. A., Simpson, J. B., & MacGregor, A. G. (1931). XIV. The igneous geology of Central Ayrshire. *Transactions of the Geological Society of Glasgow*, *18*(3), 361–386. https://doi.org/10.1144/transglas.18.3.361

Eyles, V. A., Simpson, J. B., & McGregor, A. G. (1949). Geology of central ayrshire. (Explanation of one-inch sheet 14). In *Memoirs of the Geological Survey of Scotland* (2nd ed., p. 160). HMSO. Edinburgh.

Fabricius, I. L. (2003). How burial diagenesis of chalk sediments controls sonic velocity and porosity. *AAPG Bulletin*, *87*(11), 1755–1778. https://doi.org/10.1306/06230301113

Fabricius, I. L. (2007). Chalk: Composition, diagenesis and physical properties. *Bulletin of the Geological Society of Denmark*, *55*, 97–128. https://doi.org/10.37570/bgsd-2007-55-08

Fairhead, J. D., Marsden, D., Azli, N. M., Özsöz, İ., Maxwell, D., Rose, O., & Green, C. M. (2023). Gravity imaging of sub-Zechstein geological structures in the UK sector of the North Sea using the gravity layer stripping method. *Petroleum Geoscience*, *29*(4), petgeo2023009. https://doi.org/10.1144/petgeo2023-009

Fialko, Y. A., & Rubin, A. M. (1999). Thermal and mechanical aspects of magma emplacement in giant dyke swarms. *Journal of Geophysical Research*, *104*(B10), 23033–23049. https://doi.org/10.1029/1999JB900213

Foschi, M., & Cartwright, J. (2025a). Geological property and tensile strength data for sill emplacement Study [Dataset]. *Zenodo*. https://doi.org/10.5281/zenodo.16746884

Foschi, M., & Cartwright, J. (2025b). Monte Carlo simulation code for sill emplacement pressure estimation [Software]. *Zenodo*. https://doi.org/10.5281/zenodo.16752884

Fox-Strangeways. (1992). *British geological survey 1:50,000 Sheet 43 Egton Solid Geology*. HMSO. London.

Gale, A. S., & Lovell, B. (2018). The Cretaceous–Paleogene unconformity in England: Uplift and erosion related to the Iceland mantle plume. *Proceedings of the Geologists' Association*, *129*(3), 421–435. https://doi.org/10.1016/j.pgeola.2017.04.002

Gauer, M. B., Upton, A. J., & McGrandle, A. (2004). Identification and interpretation of igneous sills in the Zechstein of the Southern North Sea Basin. Extended Abstract presented at PETEX, 23–25 November 2004, London.

Geikie, A. (1897). *The ancient volcanoes of Great Britain* (Vol. 11). McMillan. London.

Gonnermann, H., & Taisne, B. (2015). Magma transport in dikes. In *The encyclopedia of volcanoes* (pp. 215–224). Academic Press. https://doi.org/10.1016/B978-0-12-385938-9.00010-9

Green, P. F., Westaway, R., Manning, D. A. C., & Younger, P. L. (2012). Cenozoic cooling and denudation in the North Pennines (northern England, UK) constrained by apatite fission-track analysis of cuttings from the Eastgate Borehole. *Proceedings of the Geologists' Association*, *123*(3), 450–463. https://doi.org/10.1016/j.pgeola.2011.11.003

Gretener, P. E. (1969). On the mechanics of the intrusion of sills. *Canadian Journal of Earth Sciences*, *6*(6), 1415–1419. https://doi.org/10.1139/e69-143

Groome, D. R., & Hall, A. (1974). The geochemistry of the Devonian lavas of the northern Lorne Plateau, Scotland. *Mineralogical Magazine*, *39*(306), 621–640. https://doi.org/10.1180/minmag.1974.039.306.01

Grosfils, E. B. (2007). Magma reservoir failure on the terrestrial planets: Assessing the importance of gravitational loading in simple elastic models. *Journal of Volcanology and Geothermal Research*, *166*(2), 47–75. https://doi.org/10.1016/j.jvolgeores.2007.06.007

Gudmundsson, A. (2012). Magma chambers: Formation, local stresses, excess pressures, and compartments. *Journal of Volcanology and Geothermal Research*, *237*, 19–41. https://doi.org/10.1016/j.jvolgeores.2012.05.015

Gudmundsson, A. (2020). *Volcanotectonics: Understanding the structure, deformation and dynamics of volcanoes*. Cambridge University Press. https://doi.org/10.1017/9781139176217

Harris, A. L., & Pitcher, W. S. (1975). The Dalradian supergroup. In A. L. Harris, R. M. Shackleton, J. V. Watson, C. Downie, W. B. Harland, & S. Moorbath (Eds.), *A correlation of the Precambrian rocks of the British Isles* (Vol. 6, pp. 52–75). Geological Society.

Head, J. W., & Wilson, L. (1992). Magma reservoirs and neutral buoyancy zones on Venus: Implications for the formation and evolution of volcanic landforms. *Journal of Geophysical Research*, *97*(E3), 3877–3903. https://doi.org/10.1029/92JE00053

Hibsch, C., Jarrige, J. J., Cushing, E. M., & Mercier, J. (1995). Palaeostress analysis, a contribution to the understanding of basin tectonics and geodynamic evolution. Example of the Permian/Cenozoic tectonics of Great Britain and geodynamic implications in Western Europe. *Tectonophysics*, *252*(1–4), 103–136. https://doi.org/10.1016/0040-1951(95)00100-X

Holliday, D. W. (1993). Mesozoic cover over northern England: Interpretation of apatite fission track data. *Journal of the Geological Society*, *150*(4), 657–660. https://doi.org/10.1144/gsjgs.150.4.0657

Holmes, A., & Harwood, H. F. (1929). The tholeiites of the north of England. *Mineralogical Magazine and Journal of the Mineralogical Society*, *22*(124), 1–52. https://doi.org/10.1180/minmag.1929.022.124.03

Horni, J. Á., Hopper, J. R., Blischke, A., Geisler, W. H., Stewart, M., McDermott, K., et al. (2017). Regional distribution of volcanism within the North Atlantic Igneous Province. *Geological Society, London, Special Publications*, *447*(1), 105–125. https://doi.org/10.1144/SP447.18

Hubbert, M. K., & Willis, D. G. (1957). Mechanics of hydraulic fracturing. *Transactions of the AIME*, *210*(1), 153–168. https://doi.org/10.2118/686-G

Hughes, M., & Davison, I. (1993). Geometry and growth kinematics of salt pillows in the southern North Sea. *Tectonophysics*, *228*(3–4), 239–254. https://doi.org/10.1016/0040-1951(93)90343-I

Ishizuka, O., Taylor, R. N., Geshi, N., & Mochizuki, N. (2017). Large-volume lateral magma transport from the M ull volcano: An insight to magma chamber processes. *Geochemistry, Geophysics, Geosystems*, *18*(4), 1618–1640. https://doi.org/10.1002/2016GC006712

Jackson, M. P., & Hudec, M. R. (2017). *Salt tectonics: Principles and practice*. Cambridge University Press.

Japsen, P. (1998). Regional velocity-depth anomalies, North Sea Chalk: A record of overpressure and Neogene uplift and erosion. *AAPG Bulletin*, *82*(11), 2031–2074.

Jolly, R. J. H., & Sanderson, D. J. (1995). Variation in the form and distribution of dykes in the Mull swarm, Scotland. *Journal of Structural Geology*, *17*(11), 1543–1557. https://doi.org/10.1016/0191-8141(95)00046-G

Kavanagh, J. L., & Sparks, R. S. J. (2011). Insights of dyke emplacement mechanics from detailed 3D dyke thickness datasets. *Journal of the Geological Society*, *168*(4), 965–978. https://doi.org/10.1144/0016-76492010-137

Kerr, A. C., Kent, R. W., Thomson, B. A., Seedhouse, J. K., & Donaldson, C. H. (1999). Geochemical evolution of the Tertiary Mull volcano, western Scotland. *Journal of Petrology*, *40*(6), 873–908. https://doi.org/10.1093/petroj/40.6.873

Kimbell, G. S., Carruthers, R. M., Walker, A. S. D., Williamson, J. P., Busby, D. J., McDonald, A. J. W., et al. (2006). *Regional geophysics of southern Scotland and northern England*. British Geological Survey. Nottingham, UK.

Kimbell, G. S., Chadwick, R. A., Holliday, D. W., & Werngren, O. C. (1989). The structure and evolution of the Northumberland Trough from new seismic reflection data and its bearing on modes of continental extension. *Journal of the Geological Society*, *146*(5), 775–787. https://doi.org/10.1144/gsjgs.146.5.0775

Kimbell, G. S., & Williamson, J. P. (2015). A gravity interpretation of the Central North Sea. Retrieved from https://nora.nerc.ac.uk/id/eprint/516759

Kimbell, G. S., Young, B., Millward, D., & Crowley, Q. G. (2010). The North Pennine batholith (Weardale Granite) of northern England: New data on its age and form. *Proceedings of the Yorkshire Geological Society*, *58*(2), 107–128. https://doi.org/10.1144/pygs.58.1.273

Kirton, S. R., & Donato, J. A. (1985). Some buried Tertiary dykes of Britain and surrounding waters deduced by magnetic modelling and seismic reflection methods. *Journal of the Geological Society*, *142*(6), 1047–1057. https://doi.org/10.1144/gsjgs.142.6.1047

Kynaston, H., & Hill, J. B. (1908). *The geology of the country near Oban and Dalmally: (explanation of sheet 45)* (Vol. 45). HM Stationery Office.

Land, D. (1974). Geology of the Tynemouth district. In *Memoirs of the Geological Survey of Great Britain, England and Wales (Sheet—New series)*. HM Stationery Office.

Land, D. (1987). *British Geological Survey, 1:50,000 series, Stockton (Sheet 33), solid geology and drift*. HMSO. London.

Lee, G. W., & Bailey, E. B. (1925). *The pre-tertiary geology of mull, Loch aline, and oban: (being a description of parts of sheets, 35, 43, 44, 45 and 52 of the One-inch geological map of Scotland)* (Vol. 35). HM Stationery Office.

Lister, J. R., & Kerr, R. C. (1991). Fluid-mechanical models of crack propagation and their application to magma transport in dykes. *Journal of Geophysical Research*, *96*(B6), 10049–10077. https://doi.org/10.1029/91JB00600

Lorenz, V. (1986). On the growth of maars and diatremes and its relevance to the formation of tuff rings. *Bulletin of Volcanology*, *48*(5), 265–274. https://doi.org/10.1007/BF01081755

Lorenz, V. (2003). Maar-diatreme volcanoes, their formation, and their setting in hard-rock or soft-rock environments. *Geolines*, *15*, 72–83.

Lott, G. K., & Knox, R. W. O. 'B. (1994). Post-Triassic of the southern North Sea. In R. W. O. 'B. Knox & W. G. Cordey (Eds.), *Lithostratigraphic nomenclature of the UK North Sea* (Vol. 7, p. 155). British Geological Society. Keyworth, Nottingham.

Maccaferri, F., Rivalta, E., Passarelli, L., & Aoki, Y. (2016). On the mechanisms governing dike arrest: Insight from the 2000 Miyakejima dike injection. *Earth and Planetary Science Letters*, *434*, 64–74. https://doi.org/10.1016/j.epsl.2015.11.024

Macdonald, D. I. (2024). The myth of the Highland Cretaceous revealed by the art of palaeogeographic mapping. *Geological Society, London, Special Publications*, *541*(1), 347–366. https://doi.org/10.1144/SP541-2022-325

Macdonald, R., Baginski, B., Upton, B. G. J., Dzierzanowski, P., Marshall-Roberts, W., & Prieto, M. (2009). The Palaeogene Eskdalemuir dyke, Scotland: Long-distance lateral transport of rhyolitic magma in a mixed-magma intrusion. *Mineralogical Magazine*, *73*(2), 285–300. https://doi.org/10.1180/minmag.2009.073.2.285

Macdonald, R., Baginski, B., Upton, B. G. J., Pinkerton, H., MacInnes, D. A., & MacGillivray, J. C. (2010). The Mull Palaeogene dyke swarm: Insights into the evolution of the Mull igneous centre and dyke-emplacement mechanisms. *Mineralogical Magazine*, *74*(4), 601–622. https://doi.org/10.1180/minmag.2010.074.4.601

Macdonald, R., Fettes, D. J., & Bagiński, B. (2015). The Mull Paleocene dykes: Some insights into the nature of major dyke swarms. *Scottish Journal of Geology*, *51*(2), 116–124. https://doi.org/10.1144/sjg2014-016

Macdonald, R., Wilson, L., Thorpe, R. S., & Martin, A. (1988). Emplacement of the Cleveland dyke: Evidence from geochemistry, mineralogy, and physical modelling. *Journal of Petrology*, *29*(3), 559–583. https://doi.org/10.1093/petrology/29.3.559

MacGregor, A. G. (1930). Dykes of post-Carboniferous age. In *The Geology of North Ayrshire (J.E. Explanation of one inch sheet 22)*. Memoir of the Geological Survey of Great Britain. Edinburgh, Scotland.

Magee, C., Ernst, R. E., Muirhead, J., Phillips, T., & Jackson, C. A. L. (2019). Magma transport pathways in large igneous provinces: Lessons from combining field observations and seismic reflection data. In R. Srivastava, R. Ernst, & P. Peng (Eds.), *Dyke swarms of the world: A modern perspective*. Springer Geology. Springer. Singapore. https://doi.org/10.1007/978-981-13-1666-1_2

Mavko, G., Mukerji, T., & Dvorkin, J. (2020). *The rock physics handbook*. Cambridge University Press.

McLeod, P., & Tait, S. (1999). The growth of dykes from magma chambers. *Journal of Volcanology and Geothermal Research*, *92*(3–4), 231–245. https://doi.org/10.1016/s0377-0273(99)00053-0

Metropolis, N., & Ulam, S. (1949). The Monte Carlo method. *Journal of the American Statistical Association*, *44*(247), 335–341. https://doi.org/10.1080/01621459.1949.10483310

Mills, D. A. C., Hull, J. H., Burch, C. R., & Francis, E. A. (1976). *Geology of the country around Barnard Castle: Explanation of one-inch geological sheet 32, (New Series)* (Vol. 32). HM Stationery Office.

Mitchell, J. G., Rands, P. N., & Ineson, P. R. (1989). Perturbation of the K-Ar age system in the Cleveland dyke, U.K.: Evidence of an early Eocene age for barite mineralisation in the Magnesian Limestone of County Durham. *Chemical Geology*, *79*(1), 49–64. https://doi.org/10.1016/0168-9622(89)90006-7

Mondol, N. H., Fawad, M., Jahren, J., & Bjørlykke, K. (2008). Synthetic mudstone compaction trends and their use in pore pressure prediction. *First Break*, *26*(12). https://doi.org/10.3997/1365-2397.2008018

Morrison, M. A., Thompson, R. N., & Dickin, A. P. (1985). Geochemical evidence for complex magmatic plumbing during development of a continental volcanic center. *Geology*, *13*(8), 581–584. https://doi.org/10.1130/0091-7613(1985)13<581:GEFCMP>2.0.CO;2

Murase, T., & McBirney, A. R. (1973). Properties of some common igneous rocks and their melts at high temperatures. *Geological Society of America Bulletin*, *84*(11), 3563–3592. https://doi.org/10.1130/0016-7606(1973)84<3563:POSCIR>2.0.CO;2

Mykura, W., Calver, M. A., & Wilson, R. B. (1967). The Upper Carboniferous rocks of south-west Ayrshire. *Bulletin of the Geological Survey of Great Britain*, *26*, 23–98.
Parfitt, E., & Head, J., III. (1993). Buffered and unbuffered dike emplacement on Earth and Venus: Implications for magma reservoir size, depth, and rate of magma replenishment. *Earth, Moon, and Planets*, *61*(3), 249–281. https://doi.org/10.1007/BF00572247
Pharaoh, T. C. (1999). Palaeozoic terranes and their lithospheric boundaries within the Trans-European Suture Zone (TESZ): A review. *Tectonophysics*, *314*(1–3), 17–41. https://doi.org/10.1016/S0040-1951(99)00235-8
Pinel, V., & Jaupart, C. (2003). Magma chamber behavior beneath a volcanic edifice. *Journal of Geophysical Research*, *108*(B2). https://doi.org/10.1029/2002JB001751
Pinel, V., & Jaupart, C. (2004). Magma storage and horizontal dyke injection beneath a volcanic edifice. *Earth and Planetary Science Letters*, *221*(1–4), 245–262. https://doi.org/10.1016/S0012-821X(04)00076-7
Pollard, D. D. (1973). Derivation and evaluation of a mechanical model for sheet intrusions. *Tectonophysics*, *19*(3), 233–269. https://doi.org/10.1016/0040-1951(73)90021-8
Pollard, D. D., & Holzhausen, G. (1979). On the mechanical interaction between a fluid-filled fracture and the Earth's surface. *Tectonophysics*, *53*(1–2), 27–57. https://doi.org/10.1016/0040-1951(79)90353-6
Pryce, E., Cartwright, J., Kirkham, C., & Phillips, D. (2025). Sequential phreatomagmatic eruptions during the lateral propagation of giant dyke swarms. *Geology*, *53*(3), 274–278. https://doi.org/10.1130/G52490.1
Richey, J. E. (1939). The dykes of Scotland. *Transactions of the Geological Society of Edinburgh*, *13*, 393–434. https://doi.org/10.1144/transed.13.4.393
Rijkers, R., Duin, E. D., Dusar, M., & Langenaeker, V. (1993). Crustal structure of the London–Brabant massif, southern North Sea. *Geological Magazine*, *130*(5), 569–574. https://doi.org/10.1017/S0016756800020860
Rivalta, E. (2010). Evidence that coupling to magma chambers controls the volume history and velocity of laterally propagating intrusions. *Journal of Geophysical Research*, *115*(B7). https://doi.org/10.1029/2009JB006922
Rivalta, E., Taisne, B., Bunger, A. P., & Katz, R. F. (2015). A review of mechanical models of dike propagation: Schools of thought, results and future directions. *Tectonophysics*, *638*, 1–42. https://doi.org/10.1016/j.tecto.2014.10.003
Rubin, A. M. (1995). Propagation of magma-filled cracks. *Annual Review of Earth and Planetary Sciences*, *23*(1), 287–336. https://doi.org/10.1146/annurev.ea.23.050195.001443
Rubin, A. M., & Pollard, D. D. (1987). Origins of blade-like dikes in volcanic rift zones. *U. S. Geological Survey Professional Paper*, *1350*(2), 1449–1470.
Ryan, M. P. (1987). Neutral buoyancy and the mechanical evolution of magmatic systems. In B. O. Mysen (Ed.), *Magmatic processes: Physicochemical principles* (pp. 159–187). The Geochemical Society. University Park, Pa.
Ryan, M. P. (1993). Neutral buoyancy and the structure of mid-ocean ridge magma reservoirs. *Journal of Geophysical Research*, *98*(B12), 22321–22338. https://doi.org/10.1029/93JB02394
Saunders, A. D., Fitton, J. G., Kerr, A. C., Norry, M. J., & Kent, R. W. (1997). The north Atlantic igneous Province. In J. J. Mahoney & M. F. Coffin (Eds.), *Large igneous provinces: Continental, Oceanic, and planetary flood volcanism editor(s)* (Vol. 100, pp. 45–93). American Geophysical Union. https://doi.org/10.1029/GM100p0045
Scott, E. D., Wilson, L., & Head, J. W., III. (2002). Emplacement of giant radial dikes in the northern Tharsis region of Mars. *Journal of Geophysical Research*, *107*(E4), 3-1–3-10. https://doi.org/10.1029/2000JE001431
Secor, D. T., Jr., & Pollard, D. D. (1975). On the stability of open hydraulic fractures in the Earth's crust. *Geophysical Research Letters*, *2*(11), 510–513. https://doi.org/10.1029/GL002i011p00510
Smellie, W. R. (1915). The tertiary composite sill of South Bute. *Transactions of the Geological Society of Glasgow*, *15*(2), 121–139. https://doi.org/10.1144/transglas.15.2.121
Sparks, R. S. J. (2003). The dynamics of magma degassing. *Geological Society, London, Special Publications*, *v213*. https://doi.org/10.1144/GSL.SP.2003.213.01.02
Sparks, R. S. J., Meyer, P., & Sigurdsson, H. (1980). Density variation amongst mid-ocean ridge basalts: Implications for magma mixing and the scarcity of primitive lavas. *Earth and Planetary Science Letters*, *46*(3), 419–430. https://doi.org/10.1016/0012-821X(80)90055-2
Spera, F. J. (2000). Physical properties of magmas. In *Encyclopedia of volcanoes*.
Srivastava, R. K., Ernst, R. E., & Peng, P. (Eds.) (2019)., *Dyke swarms of the world: A modern perspective*. Springer. Singapore. https://doi.org/10.1007/978-981-13-1666-1
Stewart, S. A., & Coward, M. P. (1995). Synthesis of salt tectonics in the southern North Sea, UK. *Marine and Petroleum Geology*, *12*(5), 457–475. https://doi.org/10.1016/0264-8172(95)91502-G
Taisne, B., & Jaupart, C. (2009). Dike propagation through layered rocks. *Journal of Geophysical Research*, *114*(B9), B09203. https://doi.org/10.1029/2008JB006228
Thompson, R. N., Gibson, I. L., & Harmon, R. S. (1986). Two contrasting styles of interaction between basic magmas and continental crust in the British Tertiary Volcanic Province. *Journal of Geophysical Research*, *91*, 5985–5997. https://doi.org/10.1029/JB091iB06p05985
Townend, J., & Zoback, M. D. (2000). How faulting keeps the crust strong. *Geology*, *28*(5), 399–402. https://doi.org/10.1130/0091-7613(2000)28<399:HFKTCS>2.0.CO;2
Townsend, M., Pollard, D. D., & Smith, R. P. (2017). Mechanical models for dikes: A third school of thought. *Tectonophysics*, *703–4*, 98–118. https://doi.org/10.1016/j.tecto.2017.03.008
Tyrrell, G. W. (1917). Some tertiary dykes of the Clyde area. *Geological Magazine*, *4*(7), 305–315. https://doi.org/10.1017/S001675680019870X
Underhill, J. R. (2009). Role of intrusion-induced salt mobility in controlling the formation of the enigmatic "Silverpit Crater", UK Southern North Sea. *Petroleum Geoscience*, *15*(3), 197–216. https://doi.org/10.1144/1354-079309-843
Velde, B. (1996). Compaction trends of clay-rich deep sea sediments. *Marine Geology*, *133*(3–4), 193–201. https://doi.org/10.1016/0025-3227(96)00020-5
Walker, G. P. (1989). Gravitational (density) controls on volcanism, magma chambers and intrusions. *Australian Journal of Earth Sciences*, *36*(2), 149–165. https://doi.org/10.1080/08120098908729479
Wall, M., Cartwright, J., Davies, R., & McGrandle, A. (2010). 3D seismic imaging of a Tertiary Dyke Swarm in the Southern North Sea, UK. *Basin Research*, *22*(2), 181–194. https://doi.org/10.1111/j.1365-2117.2009.00416.x
Walsh, P., Boulter, M., & Morawiecka, I. (1999). Chattian and Miocene elements in the modern landscape of western Britain and Ireland. *Geological Society, London, Special Publications*, *162*(1), 45–63. https://doi.org/10.1144/GSL.SP.1999.162.01.04
Waltham, D., Taberner, C., & Docherty, C. (2000). Error estimation in decompacted subsidence curves. *AAPG Bulletin*, *84*(8), 1087–1094. https://doi.org/10.1306/A9673C3E-1738-11D7-8645000102C1865D

Williams, J. D. O., Fellgett, M. W., Kingdon, A., & Williamson, J. P. (2015). In-situ stress orientations in the UK Southern North Sea: Regional trends, deviations and detachment of the post-Zechstein stress field. *Marine and Petroleum Geology*, *67*, 769–784. https://doi.org/10.1016/j.marpetgeo.2015.06.008

Williamson, J. P., Pharaoh, T. C., Banka, D., Thybo, H., Laigle, M., & Lee, M. K. (2002). Potential field modelling of the Baltica–Avalonia (Thor–Tornquist) suture beneath the southern North Sea. *Tectonophysics*, *360*(1–4), 47–60. https://doi.org/10.1016/S0040-1951(02)00346-3

Wilson, L., & Head, J. W., III. (1981). Ascent and eruption of basaltic magma on the Earth and Moon. *Journal of Geophysical Research*, *86*(B4), 2971–3001. https://doi.org/10.1029/JB086iB04p02971

Wilson, L., & Head, J. W., III. (2002). Tharsis-radial graben systems as the surface manifeStation of plume-related dike intrusion complexes: Models and implications. *Journal of Geophysical Research*, *107*(E8), 1-1–1-24. https://doi.org/10.1029/2001JE001593

Woods, J., Winder, T., White, R. S., & Brandsdóttir, B. (2019). Evolution of a lateral dike intrusion revealed by relatively-relocated dike-induced earthquakes: The 2014–15 Bárðarbunga–Holuhraun rifting event, Iceland. *Earth and Planetary Science Letters*, *506*, 53–63. https://doi.org/10.1016/j.epsl.2018.10.032

Zadeh, M. K., Mondol, N. H., & Jahren, J. (2016). Compaction and rock properties of Mesozoic and Cenozoic mudstones and shales, northern North Sea. *Marine and Petroleum Geology*, *76*, 344–361. https://doi.org/10.1016/j.marpetgeo.2016.05.024

Zoback, M. L., Zoback, M., Watts, A., & Schubert, G. (2007). Lithosphere stress and deformation. In *Treatise on geophysics* (pp. 253–273).

References From the Supporting Information

Anderson, E. M. (1939). XVII—The dynamics of sheet intrusion. *Proceedings of the Royal Society of Edinburgh*, *58*, 242–251. https://doi.org/10.1017/s0370164600011159

Conway, A., Dentith, M. C., Doody, J. J., & Hall, J. (1987). Preliminary interpretation of upper crustal structure across the Midland Valley of Scotland from two East–West seismic refraction profiles. *Journal of the Geological Society*, *144*(6), 865–870. https://doi.org/10.1144/gsjgs.144.6.0865

Davidson, K. A. S., Sola, M., Powell, D. W., & Hall, J. (1984). Geophysical model for the Midland Valley of Scotland. *Earth and Environmental Science Transactions of the Royal Society of Edinburgh*, *75*(2), 175–181. https://doi.org/10.1017/S026359330001381X

George, T. N. (1966). Geomorphic evolution in Hebridean Scotland. *Scottish Journal of Geology*, *2*(1), 1–34. https://doi.org/10.1144/sjg02010001

Gunn, W., Clough, C. T., & Hill, J. B. (1897). *The Geology of Cowal: Including the Part of Argyllshire Between the Clyde and Loch Fine*. HM Stationery Office.

Kolano, M., Cała, M., & Stopkowicz, A. (2024). Mechanical properties of rock salt from the Kłodawa Salt Dome—A statistical analysis of geomechanical data. *Materials*, *17*(14), 3564. https://doi.org/10.3390/ma17143564

Lee, M. K., Pharaoh, T. C., Williamson, J. P., Green, C. A., & De Vos, W. (1993). Evidence on the deep structure of the Anglo-Brabant Massif from gravity and magnetic data. *Geological Magazine*, *130*(5), 575–582. https://doi.org/10.1017/S0016756800020872

Luong, M. P. (1988). Direct tensile and direct shear strengths of Fontainebleau sandstone. In *ARMA US Rock Mechanics/Geomechanics Symposium* (pp. ARMA–88). ARMA.

Pomeroy, C. D., & Morgans, W. T. A. (1956). The tensile strength of coal. *British Journal of Applied Physics*, *7*(7), 243–246. https://doi.org/10.1088/0508-3443/7/7/303

Stone, P., Millward, D., Young, B., Merritt, J. W., Clarke, S. M., McCormac, M., & Lawrence, D. J. D. (2010). *British regional geology: Northern England* (5th ed.). British Geological Survey.

Teall, J. J. H. (1884). Petrological notes on some North-of-England dykes. *Quarterly Journal of the Geological Society*, *40*(1-4), 209–247. https://doi.org/10.1144/GSL.JGS.1884.40.01-04.15

Watson, J. (1985). Northern Scotland as an Atlantic–North Sea divide. *Journal of the Geological Society*, *142*(2), 221–243. https://doi.org/10.1144/gsjgs.142.2.0221